Electronic Supplementary Information (ESI) for

Ferrocene-Templated Pd-Bearing Molecular Reactor

Artur Kasprzak*, Piotr A. Guńka

Faculty of Chemistry, Warsaw University of Technology, Noakowskiego Str. 3, 00-664 Warsaw, Poland

* corresponding author e-mail: akasprzak@ch.pw.edu.pl

Table of contents

S1. Experimental section

S1.1 Materials and methods

Chemical reagents and solvents were commercially purchased and purified according to the standard methods, if necessary. Air- and moisture-sensitive reactions were carried out using commercially anhydrous solvents under an inert atmosphere of argon. The NMR experiments were carried out using a Varian VNMRS 500 MHz spectrometer (^{1}H NMR at 500 MHz or ^{13}C NMR at 125 MHz) equipped with a multinuclear z-gradient inverse probe head. Unless otherwise stated, the spectra were recorded at 25 °C. Standard 5 mm NMR tubes were used. ^{1}H and ^{13}C chemical shifts (δ) were reported in parts per million (ppm) relative to the solvent signals: THF-d_8, δ_H (residual THF) 3.58 ppm, δ_C 67.57 ppm; DMSO-d_6, δ_H (residual DMSO) 2.50 ppm, δ_C 39.52 ppm; $CDCl_3$, δ_H (residual $CHCl_3$) 7.26 ppm, δ_C 77.23 ppm. NMR spectra were analysed with the MestReNova v12.0 software (Mestrelab Research S.L). ^{1}H DOSY (Diffusion Ordered SpectroscopY) NMR experiments were performed using a stimulated echo sequence incorporating bipolar gradient pulses[1] and with convection compensation.[2] The gradient strength was logarithmically incremented in 15 steps from 25% up to 95% of the maximum gradient strength. The DOSY Toolbox software was used for DOSY NMR spectra processing (*The DOSY Toolbox – version 2.5, 2014, Mathias Nilsson, School of Chemistry, University of Manchester, UK*). Fourier-transform infrared (FT-IR) spectra were recorded in a Attenuated Total Reflectance (ATR) mode with the Thermo Nicolet Avatar 370 spectrometer with spectral resolution of 2 cm^{-1} (100 scans). The wavenumbers for the absorption bands *v* were reported in cm^{-1}. UV-Vis and PL measurements were performed with a Cytation 3 Cell Multi-Mode Reader (BioTek Instruments, Inc.). The concentration for all the samples of native compounds was $2 \cdot 10^{-5}$ M. For the UV-Vis measurements, the wavelengths for the absorption maxima λ_{max} were reported in nm. TOF-HRMS (ESI) measurements were performed with a Q-Exactive ThermoScientific spectrometer. Elemental analyses were performed using CHNS Elementar Vario EL III apparatus. Each elemental composition was reported as an average of two analyses. Melting points were determined on Standford Research Systems MPA 100 and were uncorrected. TLC and PTLC analyses were performed using Merck Silica gel 60 F254 plates.

S1.2. Synthesis of the starting materials

Synthesis of 1,3,5-tris(4-aminophenyl)benzene

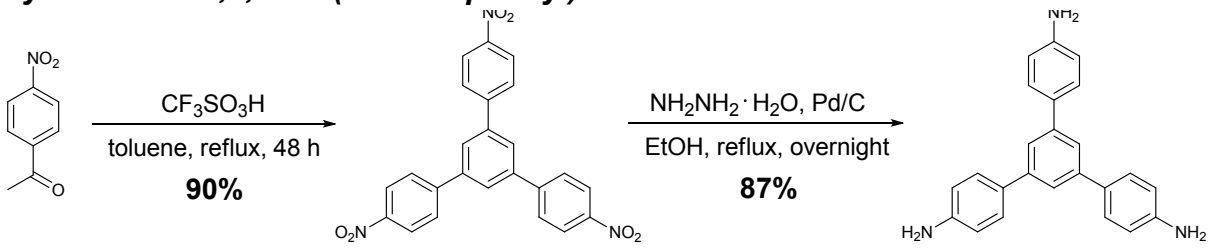

1,3,5-Tris(4-nitrophenyl)benzene and 1,3,5-tris(4-aminophenyl)benzene were synthesized based on the literature procedure.[3] A mixture of 4-nitroacetophenone

(10 g, 60.5 mmol) and triflic acid (400 µL) in toluene (40 mL) was refluxed for 48 hours. The formed black solid was filtered off and washed with toluene (15 mL). The solid was suspended in DMF (60 mL) and refluxed for 20 minutes. Hot solution was filtered off and washed with hot DMF (20 mL). The obtained solid was once again refluxed in DMF (60 mL) for 20 minutes. Filtration, washing with acetone (30 mL) and drying at 45°C for 24 hours, provided 1,3,5-tris(4-nitrophenyl)benzene (8.0114 g, 90%) as a pale-green solid. In order to obtain 1,3,5-tris(4-aminophenyl)benzene, a mixture of 1,3,5-tris(4-nitrophenyl)benzene (3 g, 6.80 mmol) and Pd/C (Pd loading 10 wt.%; 600 mg) in ethanol (60 mL) was heated to reflux and hydrazine hydrate (9 mL) was added dropwise. The resultant mixture was refluxed overnight. The reaction mixture was filtrated off trough celite and it was cooled (at -24°C for 3 hours). The formed precipitate was filtrated off and washed with cold ethanol (10 mL). The solid was dried in air for 24 hours to give 1,3,5-tris(4-aminophenyl)benzene (2.0792 g, 87%) as a bright-yellow solid. ^{1}H NMR (DMSO-d_6, 500 MHz ppm), δ_H 7.48-7.45 (m, 9H), 6.68-6.65 (m, 6H), 5.20 (bs, 6H). The NMR data is consistent with the literature.[3]

Synthesis of bis(acetonitrile)dichloropalladium(II)

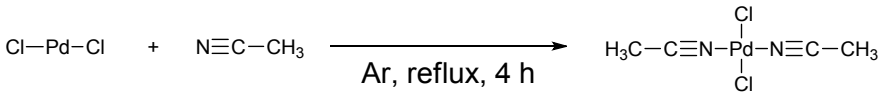

quantitative yield

Bis(acetonitrile)dichloropalladium(II) was synthesized based on the literature procedure.[4] A suspension of $PdCl_2$ (400 mg, 2.26 mmol) in dry acetonitrile (80 mL) was refluxed under argon atmosphere for 4 hours. The solvent was then evaporated on a rotary evaporator and the resultant solid was dried under high vacuum to give bis(acetonitrile)dichloropalladium(II) (586.3 mg; quantitative yield) as a yellow solid.

S1.3 Synthesis of ferrocene-templated molecular cage (3)

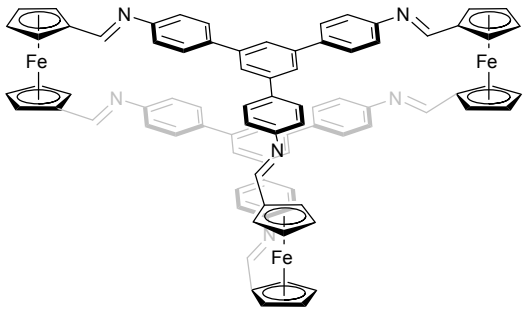

3

A solution of 1,1′-diformylferrocene (145.2 mg, 0.6 mmol) in EtOH (20 mL) was added to a solution of 1,3,5-tris(4-aminophenyl)benzene (95.9 mg, 0.4 mmol) in EtOH (10 mL). Glacial acetic acid (100 µL) was added and the mixture turned turbid. The reaction mixture was stirred at room temperature for 18 hours. Then, the formed solid was filtered off, washed with MeOH (30 mL) and dried at room temperature for 24 hours to give cage **3** (251.0 mg; 95% yield) as a dark pink solid.

Mp: >300°C; ^{1}H NMR (THF-d_8, 500 MHz, ppm), δ_H 8.15 (s, 6H), 7.49 (s, 6H), 7.30-7.28 (m, 12H), 6.81-6.78 (m, 12H), 5.06-5.05 (m, 12H), 4.50-4.51 (m, 12H); ^{13}C{^{1}H} NMR (THF-d_8, 125 MHz, ppm), δ_C 160.6 (6C), 151.2 (3C), 146.7 (3C), 141.3 (6C), 138.2 (6C), 127.5 (12C), 123.8 (6C), 120.6 (12C), 82.3 (6C), 71.7 (12C), 70.3 (12C); FT-IR (ATR), *v* 3085, 3035, 2870, 1625, 1590, 1500, 1375, 1170, 1040, 820 cm^{-1}; Elemental analysis: calculated for $C_{84}H_{60}Fe_3N_6$: C (76.38%), H (4.58%), N (6.36%), found: C (76.42%), H (4.61%), N (6.25%); TOF-HRMS (ESI): calcd. for $C_{84}H_{61}Fe_3N_6$ $[M+H]^+$ = 1321.3000, found: m/z 1321.2998.

S1.4 Interactions between the ferrocene-templated molecular cage (3) and aromatic molecules – ^{1}H NMR

The 1 mM stock solution of the ferrocene-templated molecular cage (**3**) and 8 mM stock solution of the aromatic molecule (phenylboronic acid (**G-1**), chlorobenzene (**G-2**), 1,4-terphenyl (**G-3**), chrysene (**G-4**), pyrene (**G-5**) or 1-pyrenecarboxaldehyde (**G-6**)) in THF-d_8 were prepared. The samples subjected to the NMR experiments comprised 0.5 mM (100 mol%) of the ferrocene-templated molecular cage (**3**) and 4 mM (800 mol%) of an aromatic molecule. Total volume of a sample was 0.6 mL.

S1.5 Synthesis of ferrocene-templated Pd-bearing cage (5)

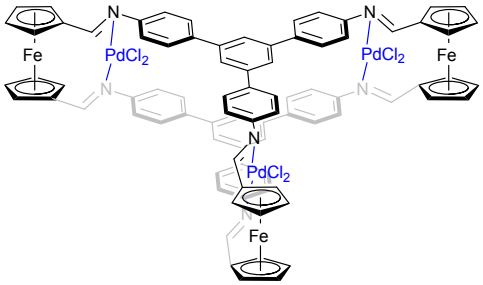

5

A solution of the ferrocene-templated molecular cage (**3**; 198.1 mg, 0.15 mmol) and bis(acetonitrile)dichloropalladium(II) (**4**; 116.8 mg, 0.45 mmol) in dry DCM (20 mL) was stirred under argon atmosphere at room temperature for 48 hours. The formed precipitate was filtered off, washed with dry DCM (30 mL) and dried under high vacuum to give cage **5** (272.4 mg; 98% yield) as a brown solid.

Mp: >300°C; ^{1}H NMR (DMSO-d_6, 500 MHz, ppm), δ_H 8.41 (s, 6H), 7.65 (s, 6H), 7.56-7.54 (m, 12H), 7.26-7.24 (m, 12H), 5.22-5.21 (m, 12H), 4.77-4.76 (m, 12H); ^{13}C{^{1}H} NMR (DMSO-d_6, 125 MHz, ppm), δ_C 168.2 (6C), 157.5 (3C), 153.3 (3C), 149.9 (6C), 142.8 (6C), 135.1 (12C), 133.4 (6C), 128.2 (12C), 90.3 (6C), 79.3 (12C), 77.6 (12C); FT-IR (ATR), *v* 3095, 3020, 2920, 1610, 1590, 1505, 1370, 1250, 1055, 830 cm-1; Elemental analysis: calculated for $C_{84}H_{60}Cl_6Fe_3N_6Pd_3$: C (54.45%), H (3.26%), N (4.54%), found: C (54.62%), H (3.43%), N (4.23%); TOF-HRMS (ESI): calcd. for $C_{84}H_{60}Cl_6Fe_3N_6Pd_3$ $[M+H]^+$ = 1853.9363, found: m/z 1853.9361.

S1.6 General procedure for the synthesis of 1,1′-biphenyls using ferrocene-templated Pd-bearing cage (5) as the catalyst

A mixture of phenylboronic acid (0.55 mmol; 110 mol%), chlorobenzene or its derivative[5] (0.50 mmol; 100 mol%), cage **5** (0.0025 mmol; **0.5 mol%**) and triethylamine (TEA; 2.00 mmol; 400 mol%) in DMSO (6 mL) was stirred at room temperature under argon atmosphere for an appropriate time[5]. The reaction progress was tracked with TLC. The mixture was diluted with hexane (35 mL) and it was cooled (at 4°C for 1 hour). The pale-red precipitate was formed, whilst the other components of the reaction mixture after a catalytic reaction remained dissolved. The solid was filtered off, washed with hexane (10 mL) and dried under high vacuum to recover catalyst as a brown solid. The compound recovered after the catalytic reaction was used as the catalyst in the next reaction cycles[5a]. The filtrate was washed with distilled water (3x15 mL), brine (2x15 mL) and dried over $MgSO_4$. After filtration, volatiles were evaporated on a rotary evaporator. The crude product was purified using PTLC (SiO_2, layer thickness of 1 μL; eluents: mixtures of AcOEt/hex) to give pure 1,1′-biphenyls in high yields (96-99%)[5b].

For the optimization of the reaction conditions for the synthesis of 1,1′-biphenyl using cage **5** as the catalyst, see **Table S1**, ESI. The proposed mechanism regarding the formation of the recovered catalyst and data for the compound recovered after the catalytic reaction (**a**) and for all the obtained 1,1′-biphenyls (**b**), are provided below. For the spectra, see Sections S7-S8, ESI.

Table S1. Optimization of the reaction conditions for the synthesis of 1,1′-biphenyl (**P-1**) using Pd-bearing cage **5** as the catalyst.

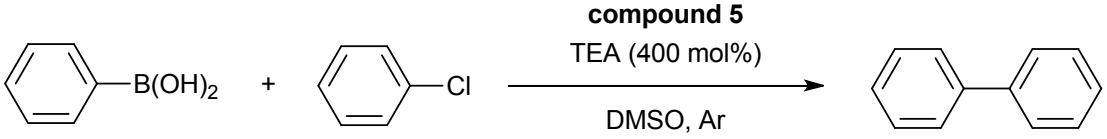

0.50 mmol (100 mol%)

P-1
95-99%

Entry	Phenylboronic acid (mol%)	Catalyst 5 (mol%)	Reaction time [minutes][a]	Reaction temperature [°C]	Yield [%][b]
1	110	10.0	20	rt	99
2	110	5.0	20	rt	99
3	**110**	**0.5**	**20**	**rt**	**99**
4	110	0.1	120	rt	98
5	110	0.5	70	90°C	95
6	130	0.5	20	rt	99

[a] the reaction progress was tracked with TLC; [b] isolated yields.

a) ^{1}H NMR, ^{13}C NMR, elemental analysis and melting point data for the compound recovered after the catalytic reaction (NMR spectra are presented in Section S8, ESI):

The data on the compound recovered after the catalytic reaction are as follows:

Mp: >300°C; ^{1}H NMR (DMSO-d_6, 500 MHz, ppm), δ_H 8.41 (s, 6H), 7.65 (s, 6H), 7.56-7.54 (m, 12H), 7.26-7.24 (m, 12H), 5.22-5.21 (m, 12H), 4.77-4.76 (m, 12H); ^{13}C{^{1}H} NMR (DMSO-d_6, 125 MHz, ppm), δ_C 167.5 (6C), 157.5 (3C), 153.0 (3C), 149.9 (6C), 142.8 (6C), 135.1 (12C), 133.4 (6C), 128.2 (12C), 90.3 (6C), 79.2 (12C), 77.5 (12C); Elemental analysis: found: C (61.68%), H (3.57%), N (5.18%); TOF-HRMS (ESI): found: m/z 1639.0032.

Based on above-presented data, the Pd^0[cage] was isolated after the catalytic process (elemental analysis: calculated for $C_{84}H_{60}Fe_3N_6Pd_3$: C (61.51%), H (3.69%), N (5.12%); HRMS: calcd. for $C_{84}H_{60}Fe_3N_6Pd_3$ $[M]^+$ = 1639.0039).

In fact, the cage comprising the Pd^0 acted the catalyst in the catalytic process. The following mechanism for the generation of Pd^0[cage] from Pd^{II}Cl$_2$[cage] is proposed[5c]:

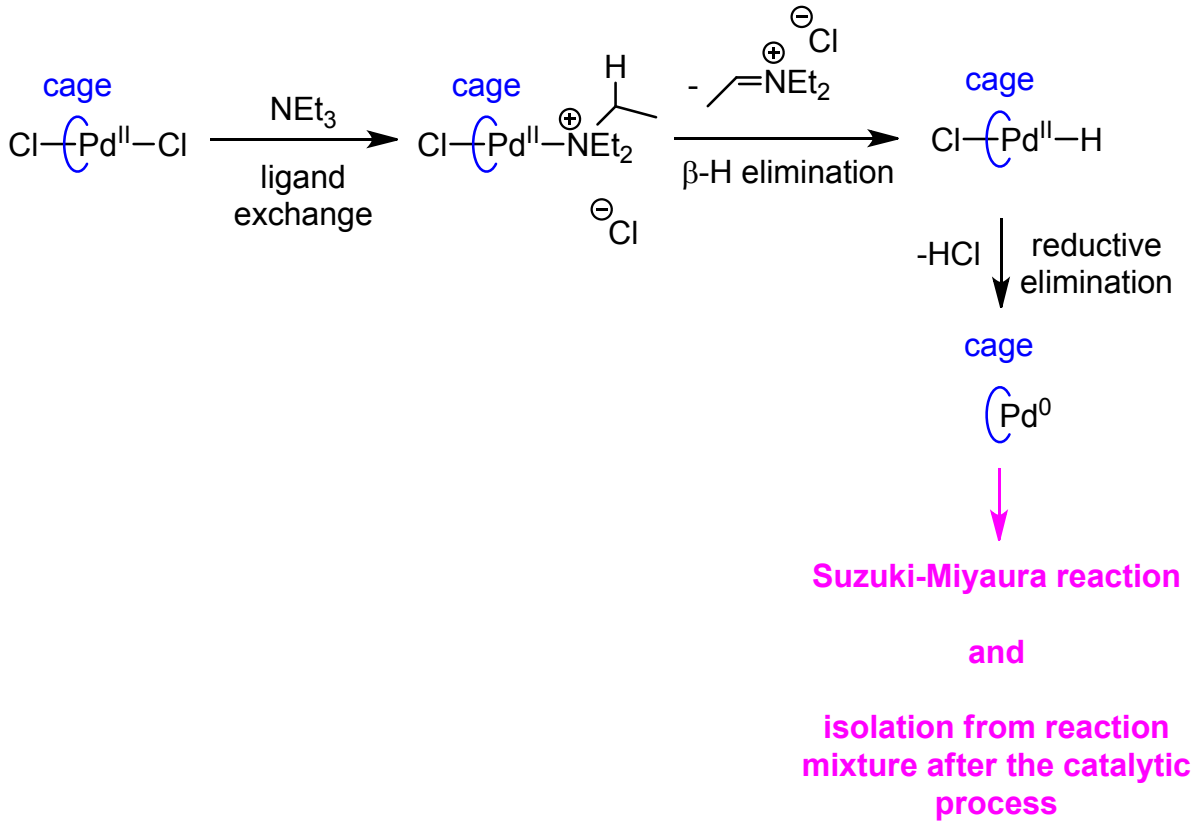

b) ^{1}H NMR, HRMS and melting point data for the 1,1′-biphenyls obtained in the catalytic reaction (^{1}H NMR spectra are presented in Section S7, ESI). The data for all the obtained 1,1′-biphenyls are consistent with the literature.[6],[7]

*1,1'-biphenyl (**P-1**):*

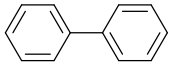

P-1

Yield[8] (0.50 mmol scale): **99 %**; Yield[8] (10.00 mmol scale): **99 %**.
Reaction time (0.50 mmol scale): **20 minutes**; Reaction time (10.00 mmol scale): **21 minutes**.
Mp: 70°C; ^{1}H NMR ($CDCl_3$, 500 MHz, ppm), δ_H 7.63-7.61 (m, 4H), 7.48-7.44 (m, 4H), 7.39-7.35 (m, 2H); TOF-HRMS (ESI): calcd. for $C_{12}H_{10}$ $[M]^+$ = 154.0783, found: m/z 154.0782. No differences between the spectra of 1,1′-biphenyl obtained in 0.50 mmol and 10.00 mmol scale reactions, were found.

*4-methyl-1,1'-biphenyl (**P-2**):*

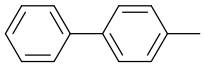

P-2

Yield[8]: **98 %**.
Reaction time: **21 minutes**.
Mp: 46°C; ^{1}H NMR ($CDCl_3$, 500 MHz, ppm), δ_H 7.61-7.58 (m, 2H), 7.53-7.50 (m, 2H), 7.46-7.42 (m, 2H), 7.36-7.32 (m, 1H), 7.28-7.26 (m, 2H), 2.42 (s, 3H); TOF-HRMS (ESI): calcd. for $C_{13}H_{12}$ $[M]^+$ = 168.0939, found: m/z 168.0941.

*4-nitro-1,1'-biphenyl (**P-3**):*

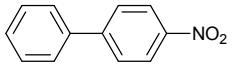

P-3

Yield[8]: **96 %**.
Reaction time: **26 minutes**.
Mp: 113°C; ^{1}H NMR ($CDCl_3$, 500 MHz, ppm), δ_H 8.32-8.30 (m, 2H), 7.75-7.73 (m, 2H), 7.51-7.40 (m, 5H); TOF-HRMS (ESI): calcd. for $C_{13}H_9NO_2$ $[M]^+$ = 199.0633, found: m/z 199.0631.

*4-bromo-1,1'-biphenyl (**P-4**):*

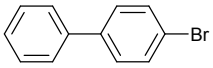

P-4

Yield[8]: **97 %**.
Reaction time: **23 minutes**.
Mp: 89°C; ^{1}H NMR ($CDCl_3$, 500 MHz, ppm), δ_H 7.59-7.56 (m, 4H), 7.48-7.43 (m, 4H), 7.39-7.36 (m, 1H); TOF-HRMS (ESI): calcd. for $C_{12}H_9Br$ $[M]^+$ = 231.9888, found: m/z 231.9885.

*2-bromo-1,1'-biphenyl (**P-5**):*

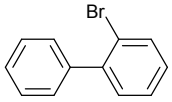

P-5

Yield[8]: **96 %**.
Reaction time: **25 minutes**.
Bright-yellow liquid; ^{1}H NMR ($CDCl_3$, 500 MHz, ppm), δ_H 7.70-7.68 (m, 1H), 7.46-7.34 (m, 7H), 7.24-7.19 (m, 1H); TOF-HRMS (ESI): calcd. for $C_{12}H_9Br$ $[M]^+$ = 231.9888, found: m/z 231.9887.

S2. NMR spectra

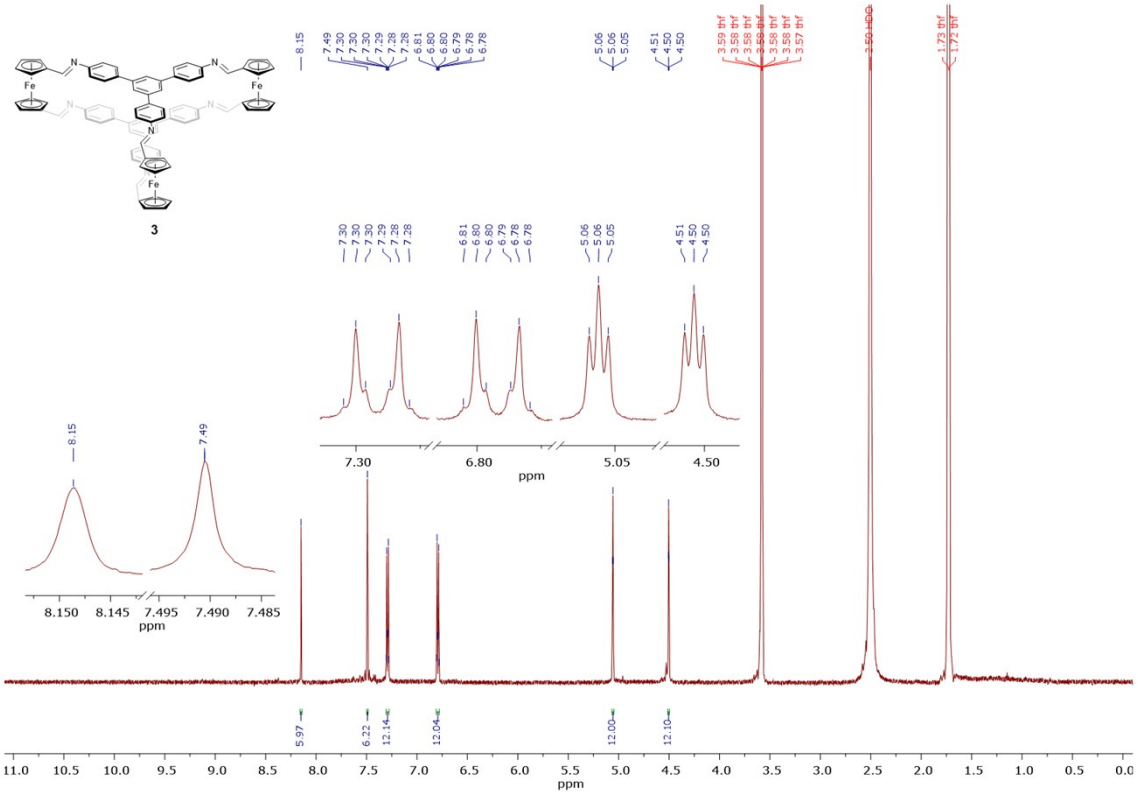

Figure S1. ^{1}H NMR (THF-d_8, 500 MHz) spectrum of cage **3**.

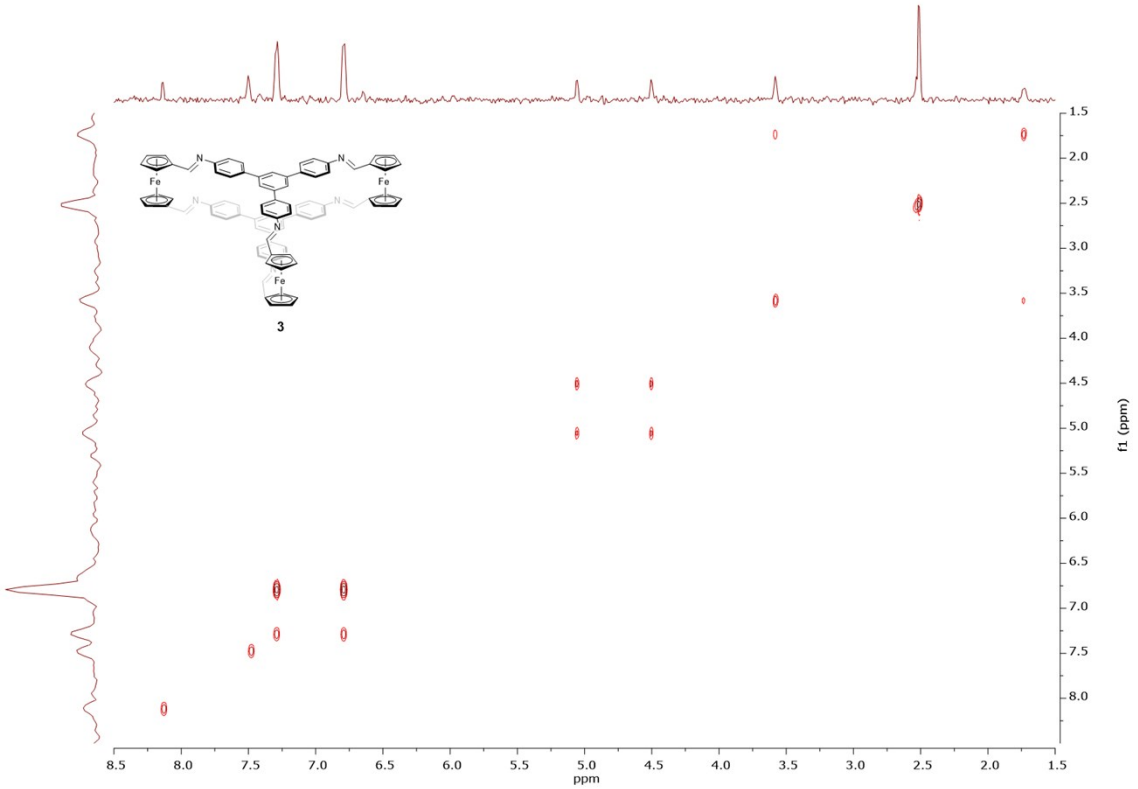

Figure S2. ^{1}H-^{1}H COSY NMR (THF-d_8, 500 MHz) spectrum of cage **3**.

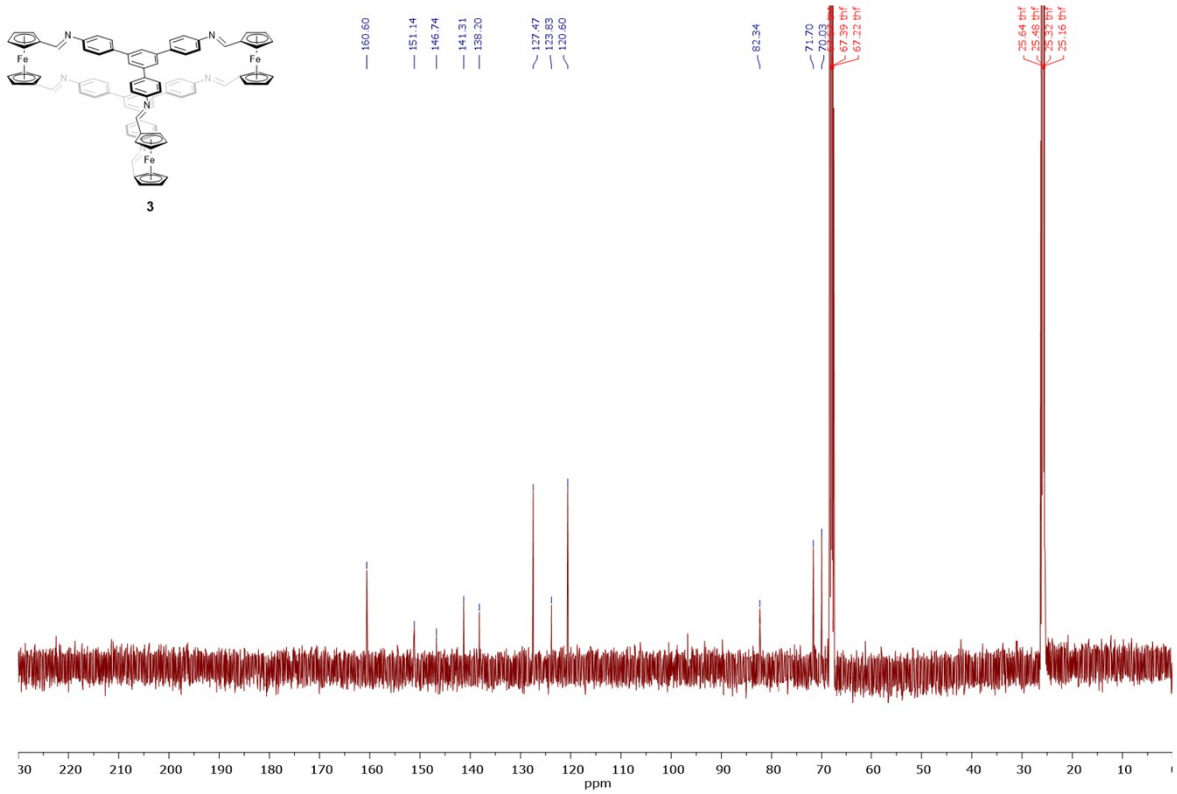

Figure S3. ^{13}C NMR (THF-d_8, 125 MHz) spectrum of cage **3**.

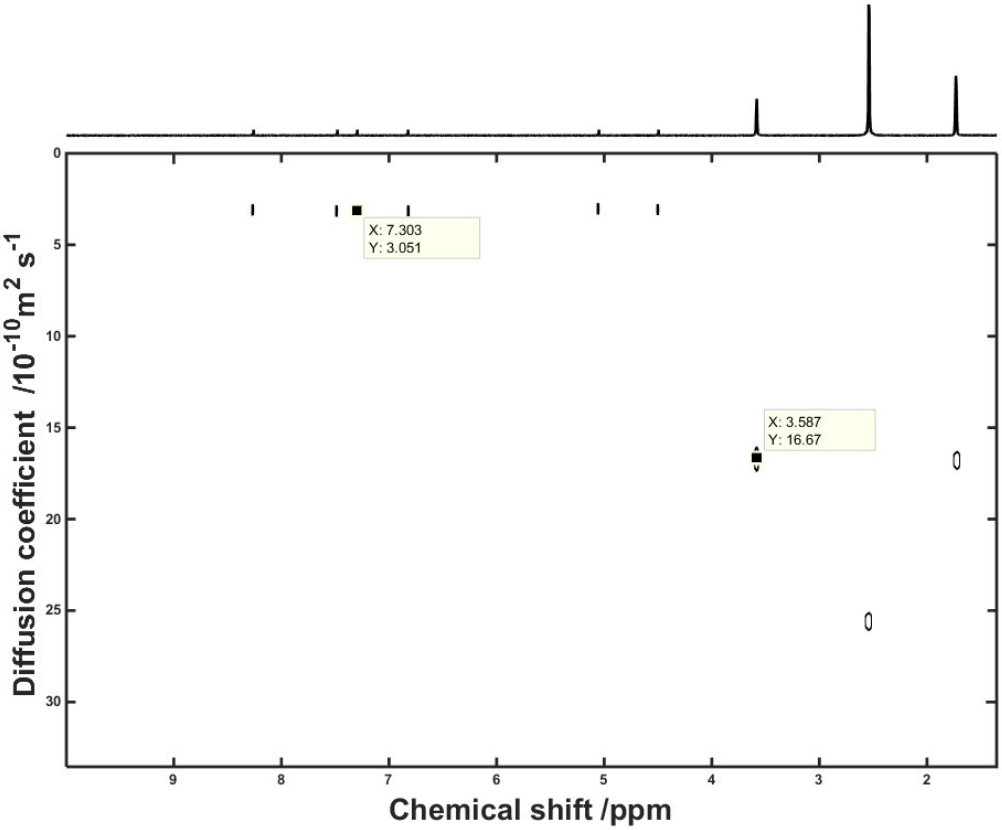

Figure S4. ^{1}H DOSY NMR (THF-d_8, 500 MHz) spectrum of cage **3**.

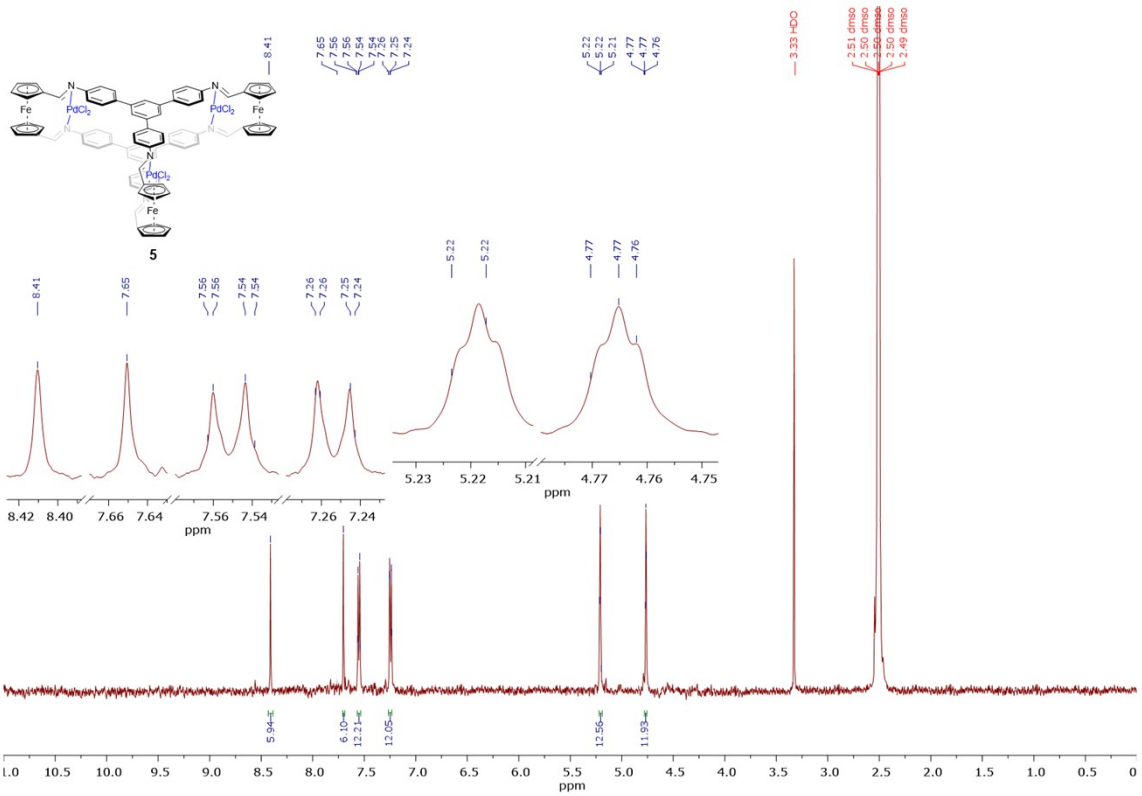

Figure S5. ^{1}H NMR (DMSO-d_6, 500 MHz) spectrum of cage **5**.

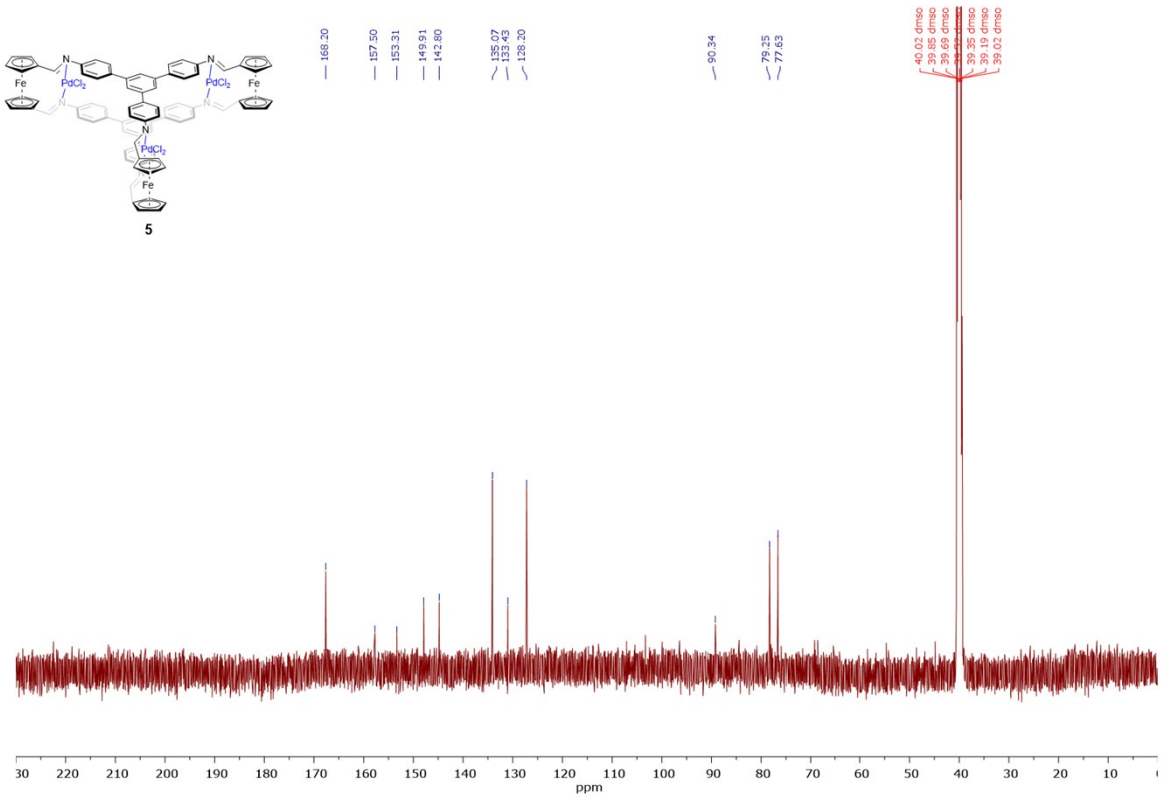

Figure S6. ^{13}C NMR (DMSO-d_6, 125 MHz) spectrum of cage **5**.

S3. IR spectra

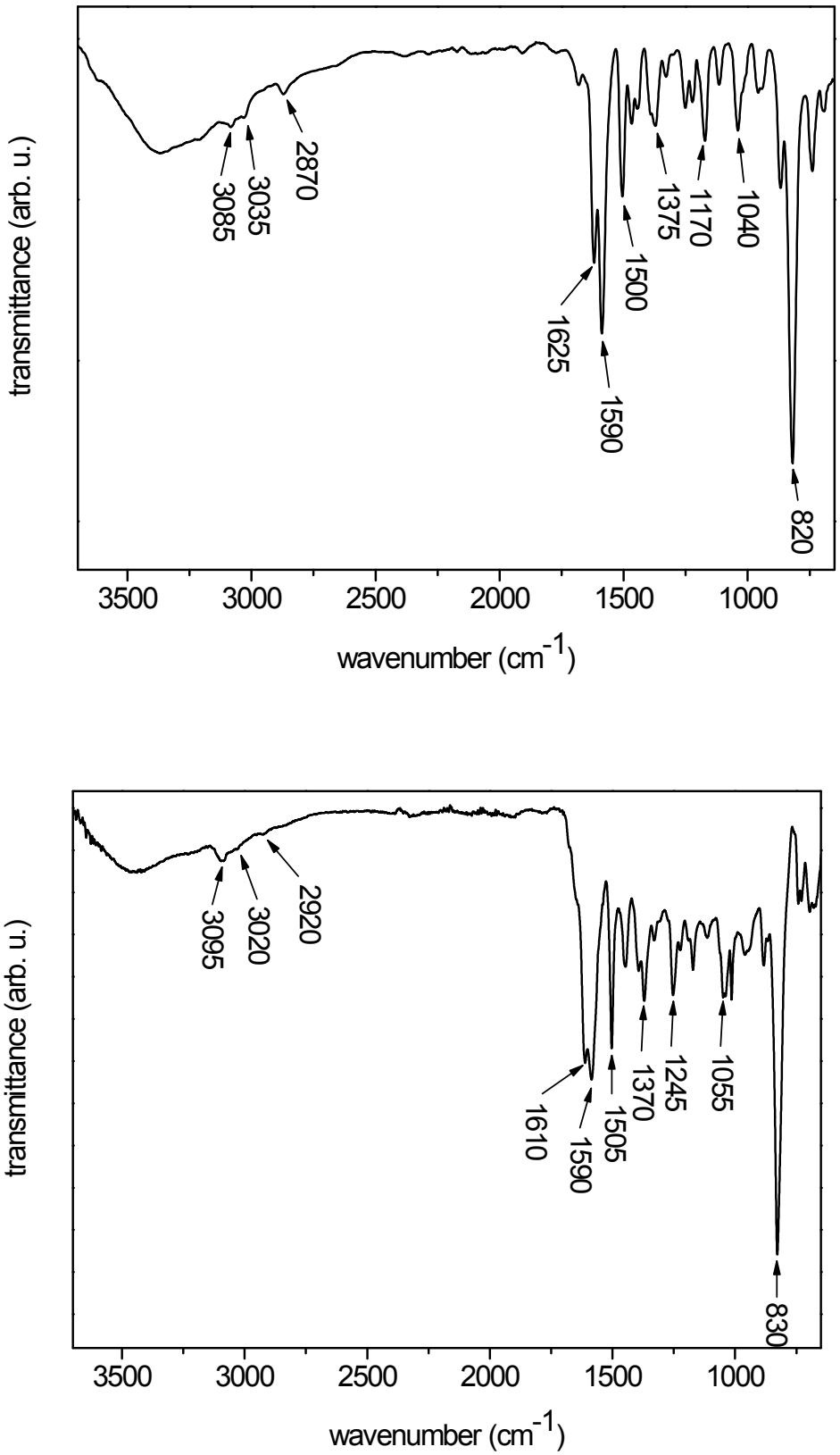

Figure S7. FT-IR spectrum of cage **3** (**top**) and cage **5** (**bottom**).

S4. UV-Vis spectra for compound 3 and compound 5

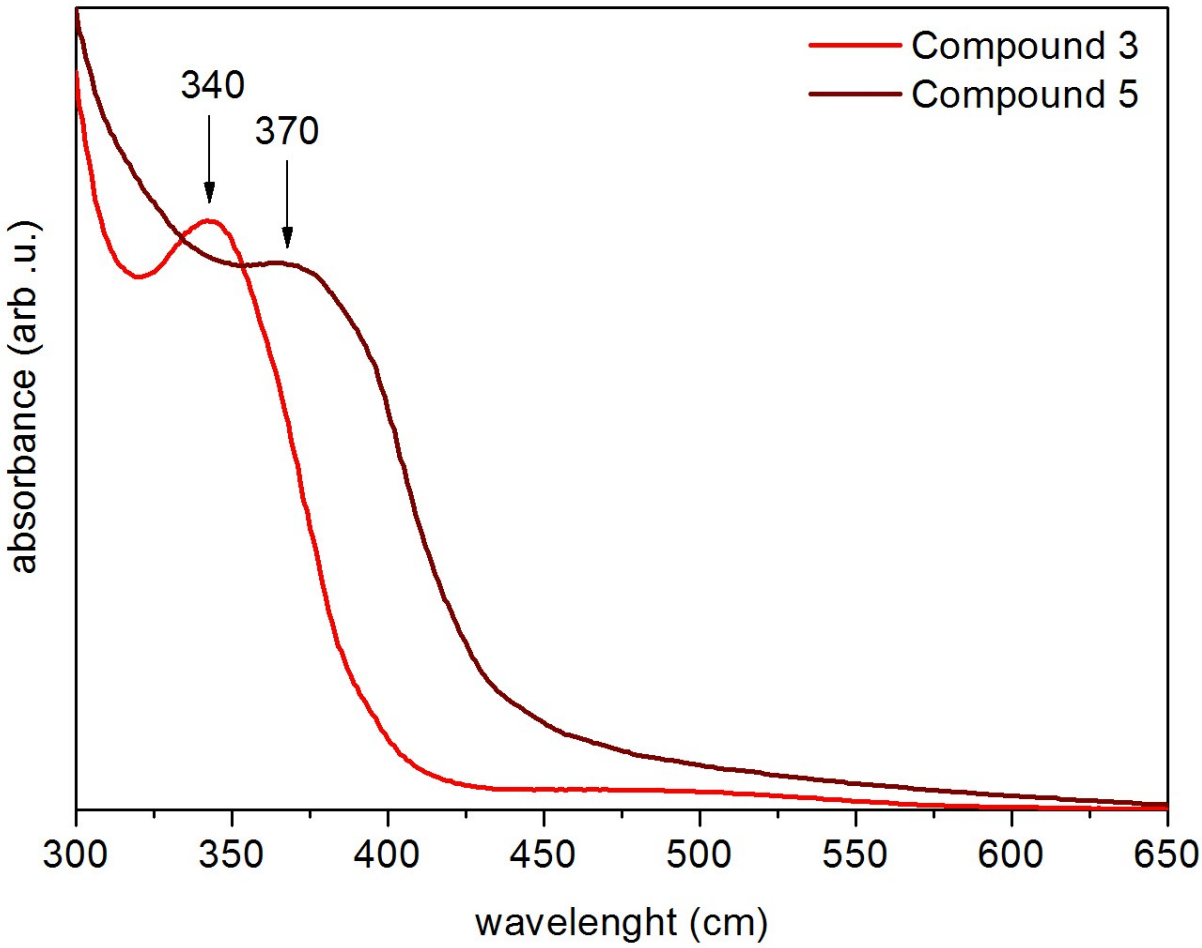

Figure S8. UV-Vis spectra of cage **3** (**red curve:** solvent: THF, concentration: $2 \cdot 10^{-5}$ M) and cage **5** (**brown curve:** solvent: DMSO, concentration: $2 \cdot 10^{-5}$ M).

S5. Crystal structure analyses on cage 3

Single crystals of cage **3** suitable for crystal structure determination were grown after five days of slow evaporation of a dichloromethane solution of cage **3** with a layer of benzene on top of it. Appropriate single crystal for X-ray diffraction experiment was selected under a microscope using polarized light and attached to a cactus needle with a two-component epoxy glue. Diffraction data were collected using graphite-monochromated Mo-Kα X-ray radiation on a Rigaku Oxford Diffraction Gemini A Ultra diffractometer equipped with Atlas CCD detector. CrysAlis^{PRO} software was used for data collection and analysis.[9] Crystal structure was subsequently solved and refined using ShelxT and ShelxL programs, respectively, invoked from within Olex2 suite.[10]-[12] Hydrogen atoms were introduced into calculated positions. The crystal structure contains two types of voids. The smaller ones with a volume of 216 Å^3 are centered at 3*b* Wyckoff position (0, 0, ½; symmetry of $\bar{3}$ point group) and the larger ones (223 Å^3) are located at 9*d* Wyckoff position (½, 0, ½; symmetry of $\bar{1}$ point group). The larger voids are occupied by benzene molecules as evidenced by the Q-peaks in residual density maps whereas the smaller ones are probably occupied by dichloromethane molecules. This is inferred based on the cavities' shape which is more isotropic than that of the larger voids. The final model of the structure was obtained by removing the contribution of all the disordered solvent molecules from scattering factors by the SQUEEZE procedure implemented in PLATON.[13,][14] The number of "squeezed" electrons is 62 and 52 for the larger and smaller voids, respectively. This is more than 42 which is the number of benzene and dichloromethane electrons but SQUEEZE is known to overestimate the number of solvent molecule electrons.[14] Details of crystal structure determination are given in **Table S2**. CCDC 1970365 contains supplementary crystallographic data for this paper. These data can be obtained free of charge from the joint CCDC's and FIZ Karlsruhe's service to view and retrieve structures via https://www.ccdc.cam.ac.uk/structures/.

Table S2. Crystal data and structure refinement for cage **3**.

Identification code	Cage **3**
Empirical formula	$C_{84}H_{60}Fe_3N_6$
Formula weight	1320.93
T /K	293.15
Crystal system	trigonal
Space group	$R\bar{3}$
a /Å	24.9627(11)
b /Å	24.9627(11)
c /Å	20.5795(11)
α /°	90
β /°	90
γ /°	120
V /Å^3	11105.8(11)
Z	6
ρ_{calc}/g/cm^3	1.185
μ/mm^{-1}	0.626
F(000)	4104.0
Crystal size/mm^3	0.25 × 0.19 × 0.085
Radiation	MoKα (λ = 0.71073)
2Θ range for data collection/°	6.778 to 53.998
Index ranges	−29 ≤ *h* ≤ 27, −24 ≤ *k* ≤ 31, −20 ≤ *l* ≤ 26
Reflections collected	11433
Independent reflections	5389 [R_{int} = 0.0362, R_{sigma} = 0.0644]
Data/restraints/parameters	5389/0/280
Goodness-of-fit on F^2	0.964
Final *R* indexes [*I*>=2σ (*I*)]	R_1 = 0.0467, wR_2 = 0.0982
Final *R* indexes [all data]	R_1 = 0.0854, wR_2 = 0.1154
Largest diff. peak/hole / eÅ^{-3}	+0.35/−0.19

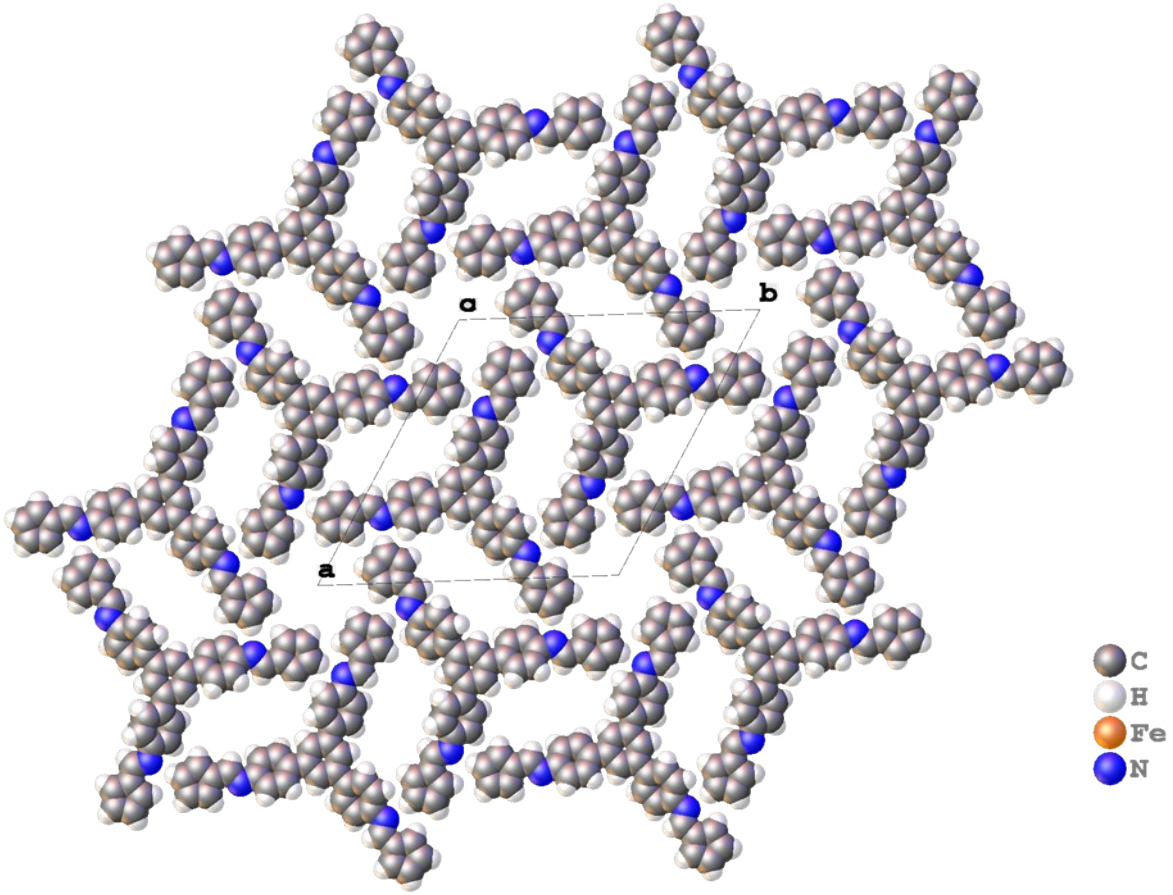

Figure S9. View of one layer of molecules along crystallographic *c* direction in cage **3** crystal structure. Molecules drawn in space-filling model. See legend for colour coding of atoms. The larger and smaller voids contain disordered solvent molecules of benzene and dichloromethane, respectively.

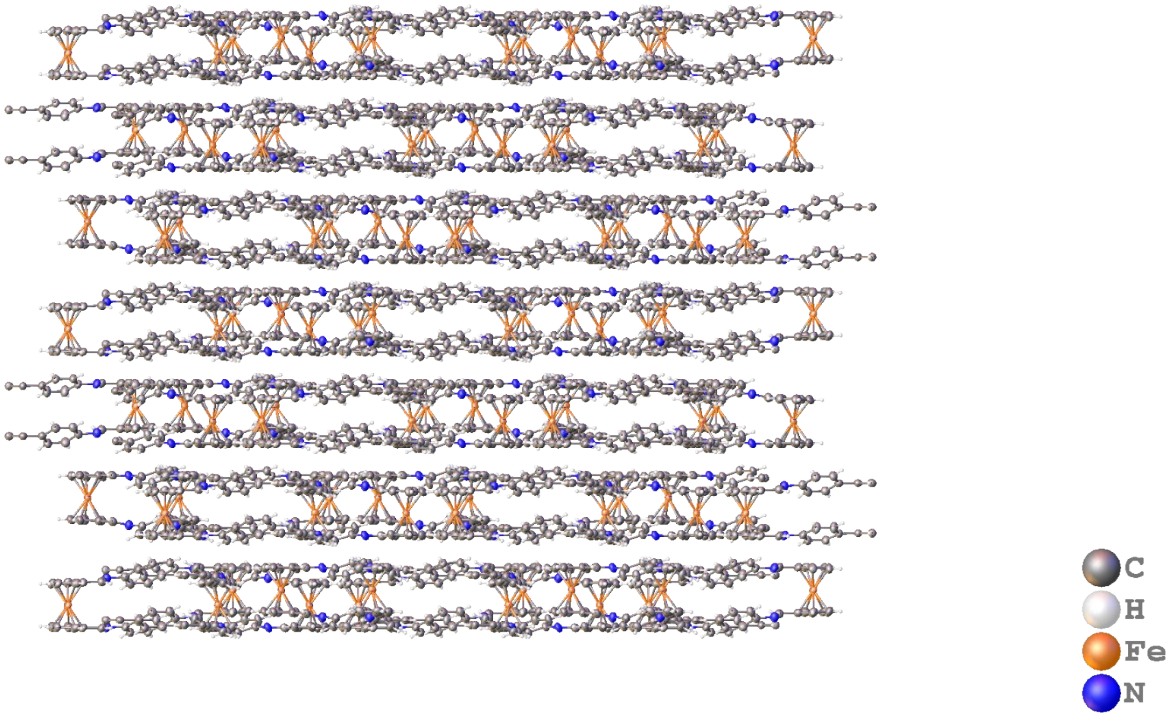

Figure S10. View of 3D packing of molecules along crystallographic *a* direction in cage **3** crystal structure. Molecules drawn ellipsoids representing thermal motion of 50% probability level. See legend for colour coding of atoms. The larger and smaller voids contain disordered solvent molecules of benzene and dichloromethane, respectively.

S6. Interactions with aromatic molecules – NMR assays

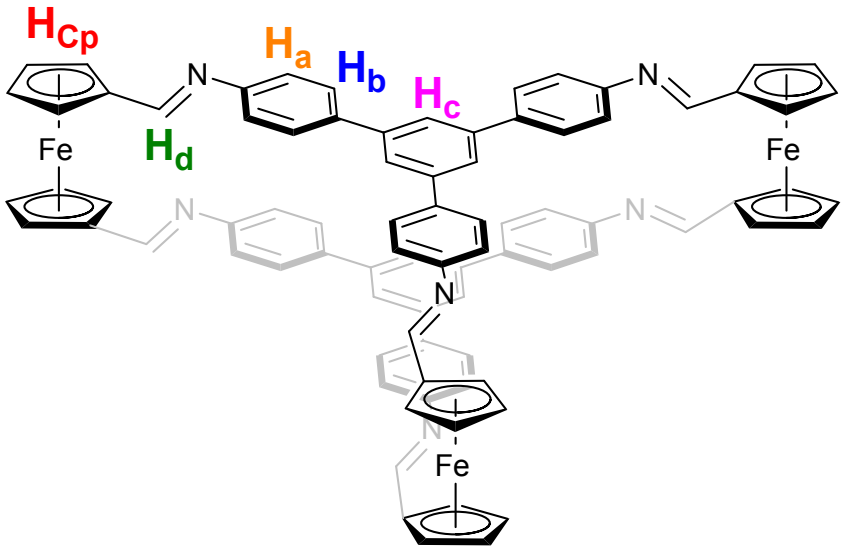

3

Figure S11. Structure of the molecular cage **3** with the atom labels marked.

Table S3. Relative signal shifts for the H_b protons of cage **3** after the addition of 800 mol% of an aromatic molecule. No shift for the H_{cp} and H_d protons were observed (see the spectra below). For the atom labels of cage **3**, see Figure S11. For the structures of the aromatic molecules, see Figure 2 in the main article text.

Entry	Aromatic molecule	Chemical shift for H_b (ppm)	Relative difference in the chemical shift in comparison to native cage 3 (ppm)
1	- (native cage **3**)	6.810	N/A
2	phenylboronic acid (**G-1**)	6.761	-0.049
3	chlorobenzene (**G-2**)	6.763	-0.047
4	1,4-terphenyl (**G-3**)	6.789	-0.021
5	chrysene (**G-4**)	6.782	-0.028
6	pyrene (**G-5**)	6.778	-0.032
7	1-pyrenecarboxaldehyde (**G-6**)	6.732	-0.078

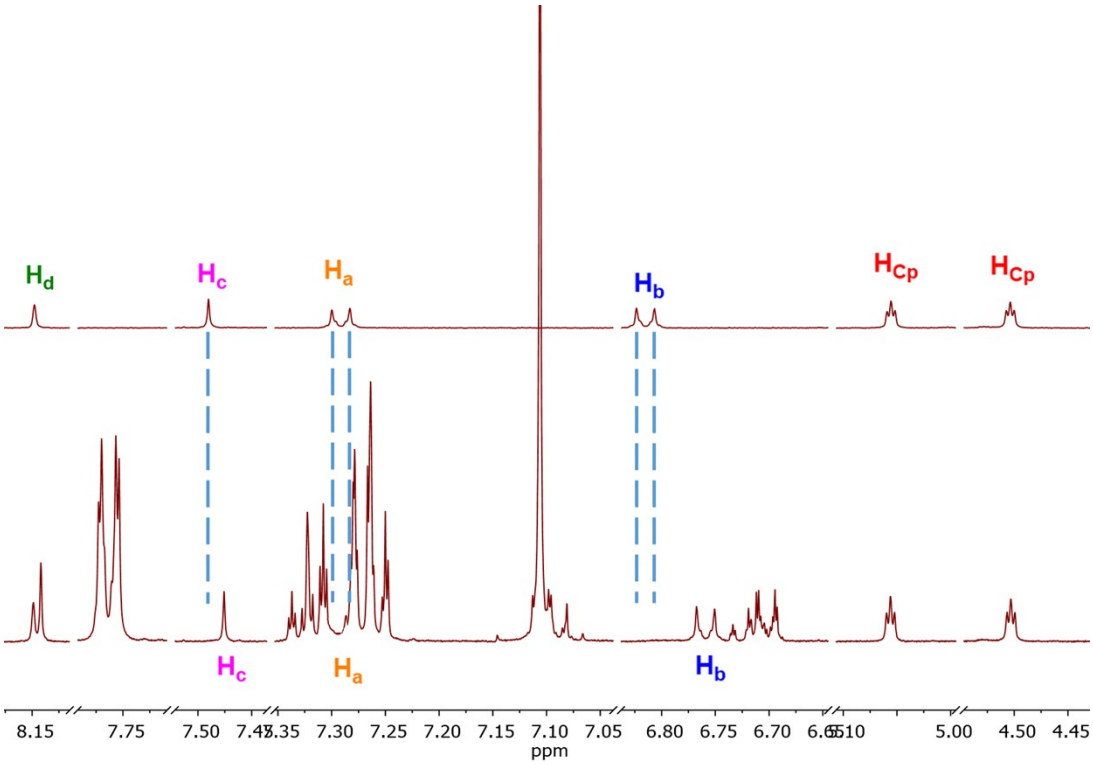

Figure S12. ^{1}H NMR (THF-d_8, 500 MHz) spectrum of cage **3** (**top**) and ^{1}H NMR (THF-d_8, 500 MHz) spectrum of cage **3** with 800 mol% of phenylboronic acid (**G-1**) added (**bottom**). For the atom labels of cage **3**, see Figure S11.

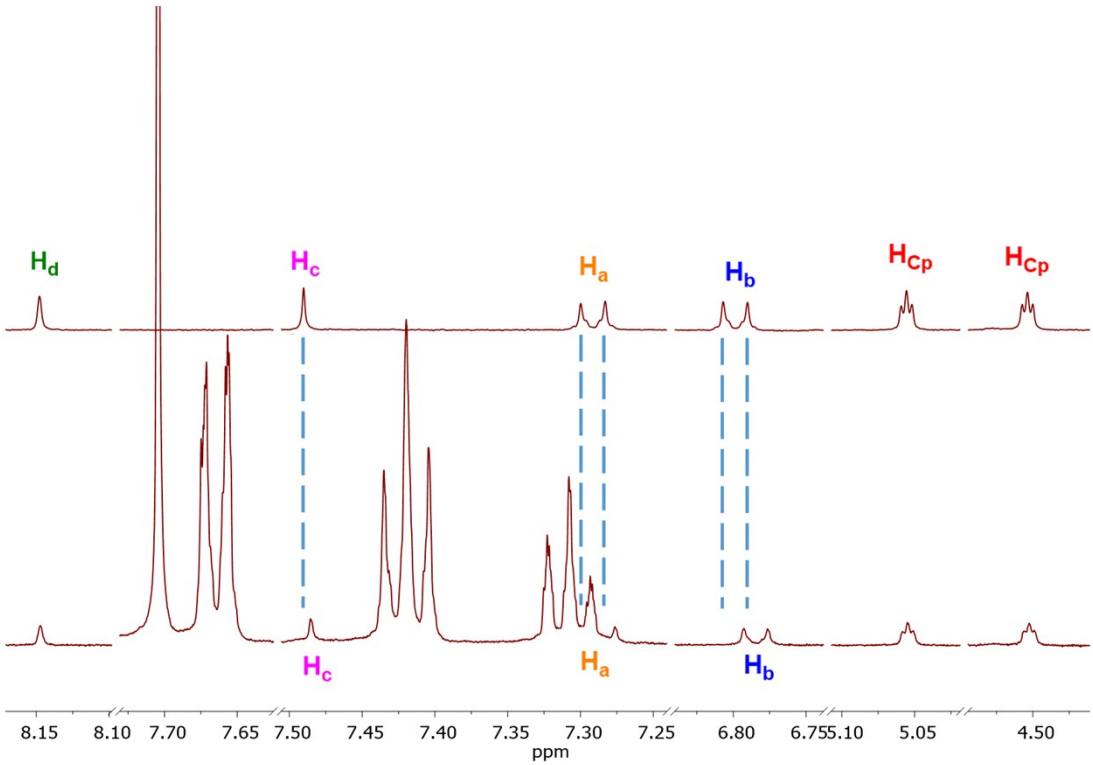

Figure S13. ^{1}H NMR (THF-d_8, 500 MHz) spectrum of cage **3** (**top**) and ^{1}H NMR (THF-d_8, 500 MHz) spectrum of cage **3** with 800 mol% of 1,4-terphenyl (**G-3**) added (**bottom**). For the atom labels of cage **3**, see Figure S11.

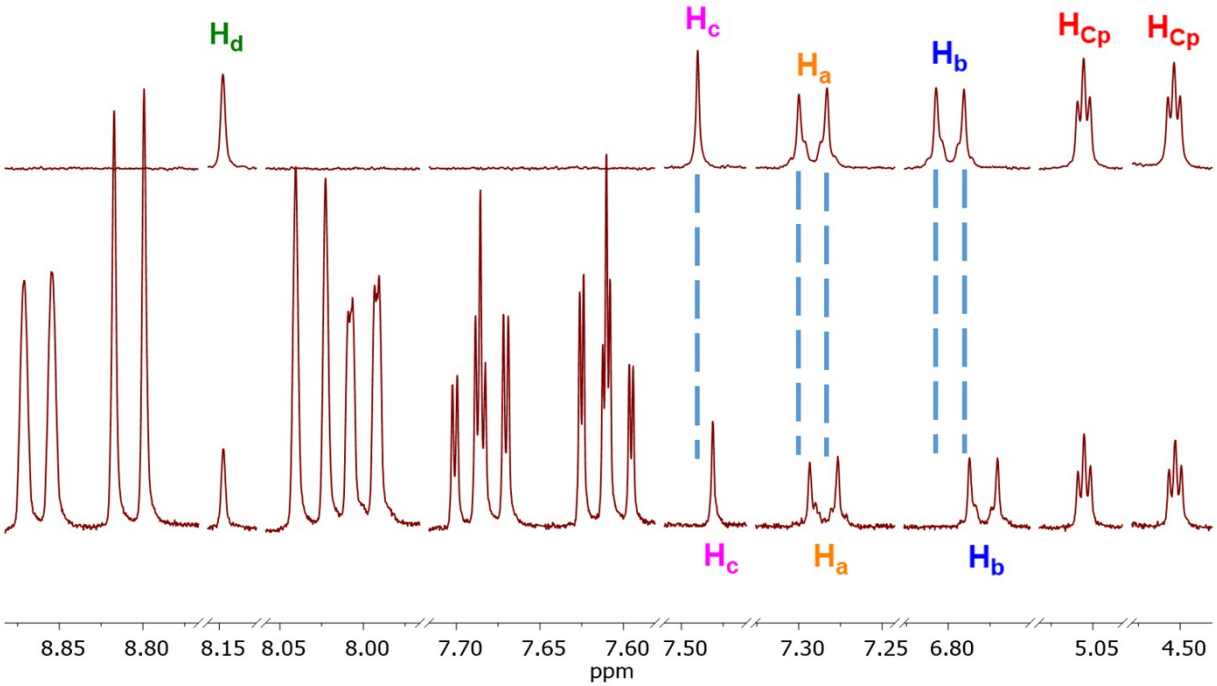

Figure S14. ^{1}H NMR (THF-d_8, 500 MHz) spectrum of cage **3** (**top**) and ^{1}H NMR (THF-d_8, 500 MHz) spectrum of cage **3** with 800 mol% of chrysene (**G-4**) added (**bottom**). For the atom labels of cage **3**, see Figure S11.

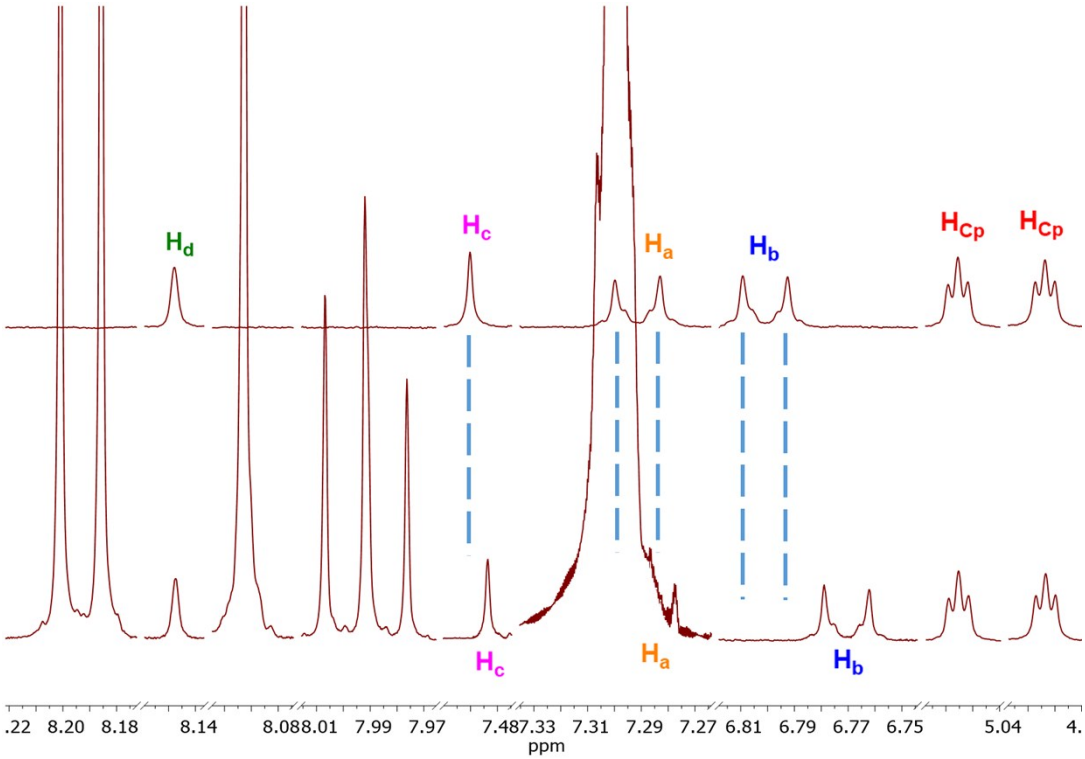

Figure S15. ^{1}H NMR (THF-d_8, 500 MHz) spectrum of cage **3** (**top**) and ^{1}H NMR (THF-d_8, 500 MHz) spectrum of cage **3** with 800 mol% of pyrene (**G-5**) added (**bottom**). For the atom labels of cage **3**, see Figure S11.

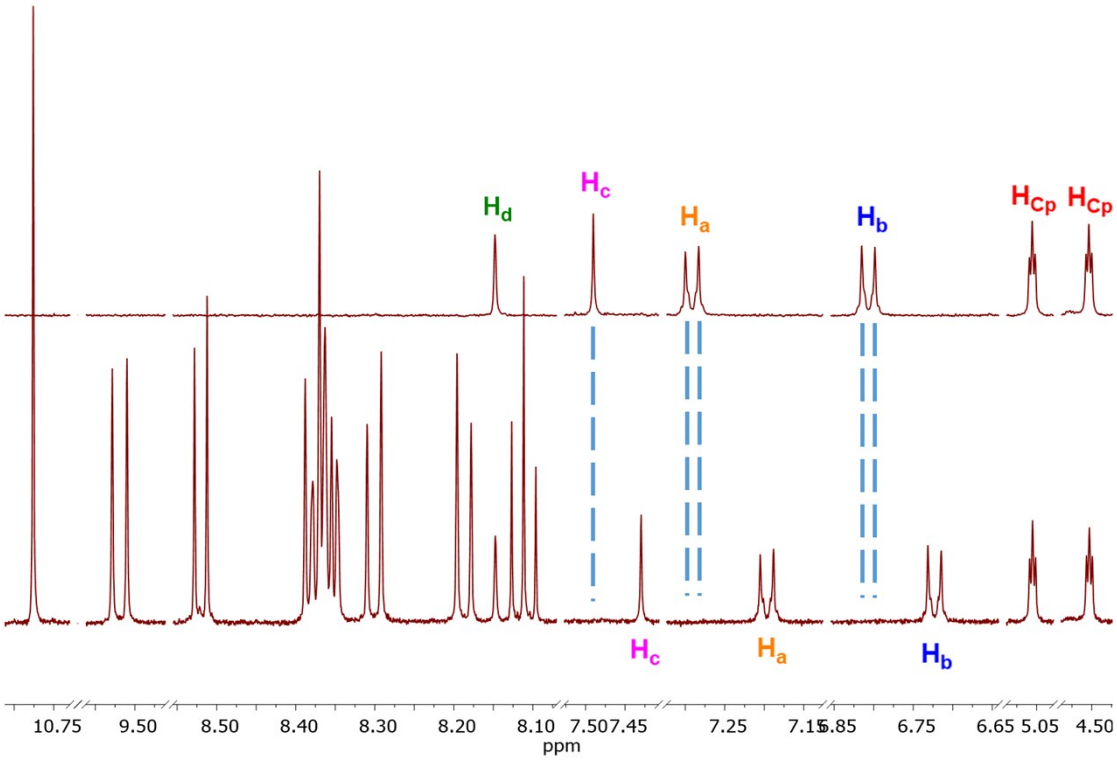

Figure S16. ^{1}H NMR (THF-d_8, 500 MHz) spectrum of cage **3** (**top**) and ^{1}H NMR (THF-d_8, 500 MHz) spectrum of cage **3** with 800 mol% of 1-pyrenecarboxaldehyde (**G-6**) added (**bottom**). For the atom labels of cage **3**, see Figure S11.

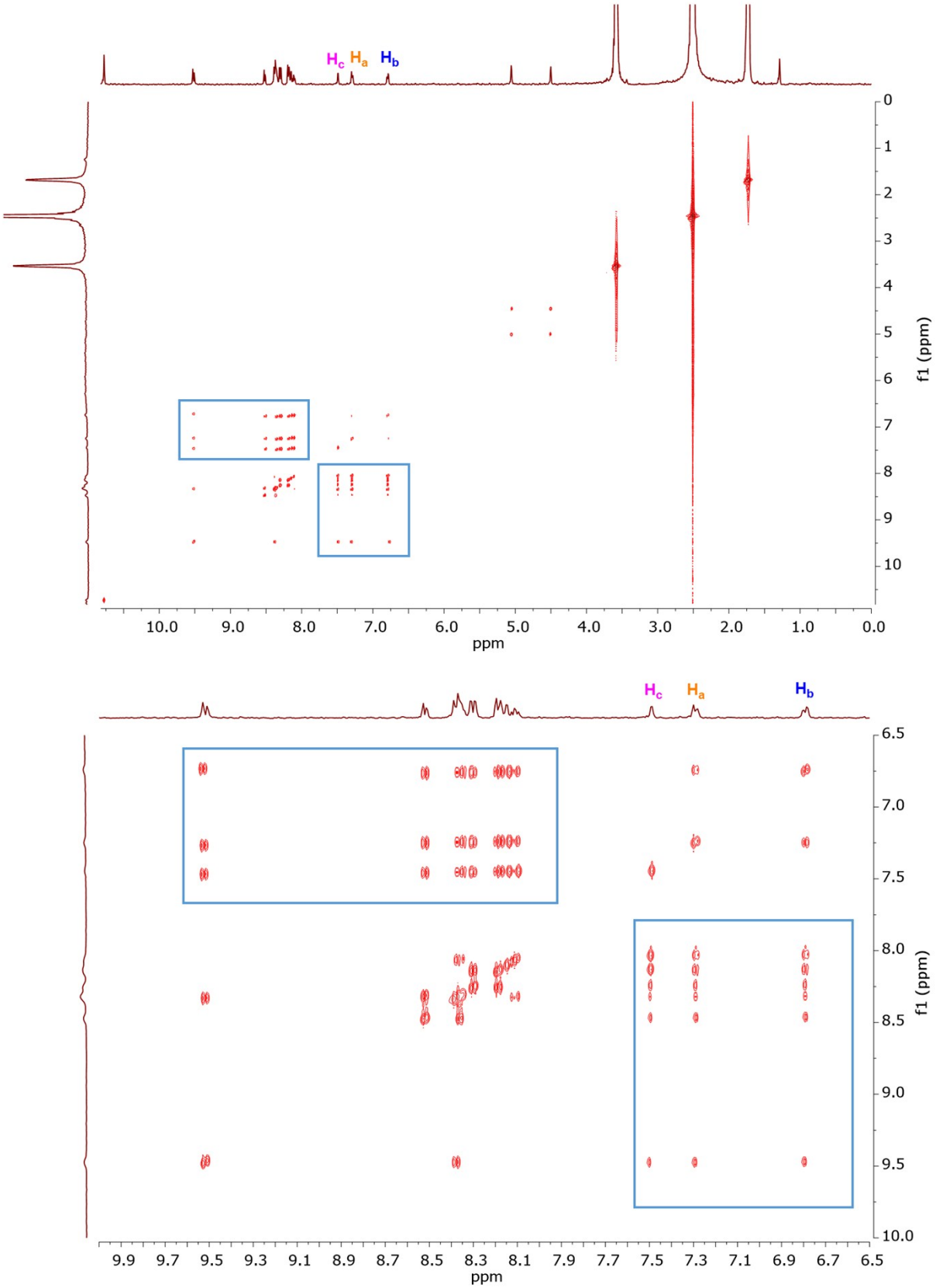

Figure S17. ^{1}H-^{1}H ROESY NMR (THF-d_8, 500 MHz) spectrum of cage **3** with 800 mol% of 1-pyrenecarboxaldehyde (**G-6**) added (top) and 10.00-6.50 ppm inset of this spectrum (**bottom**). The crucial cross-correlations are marked in blue. For the atom labels of cage **3**, see Figure S11.

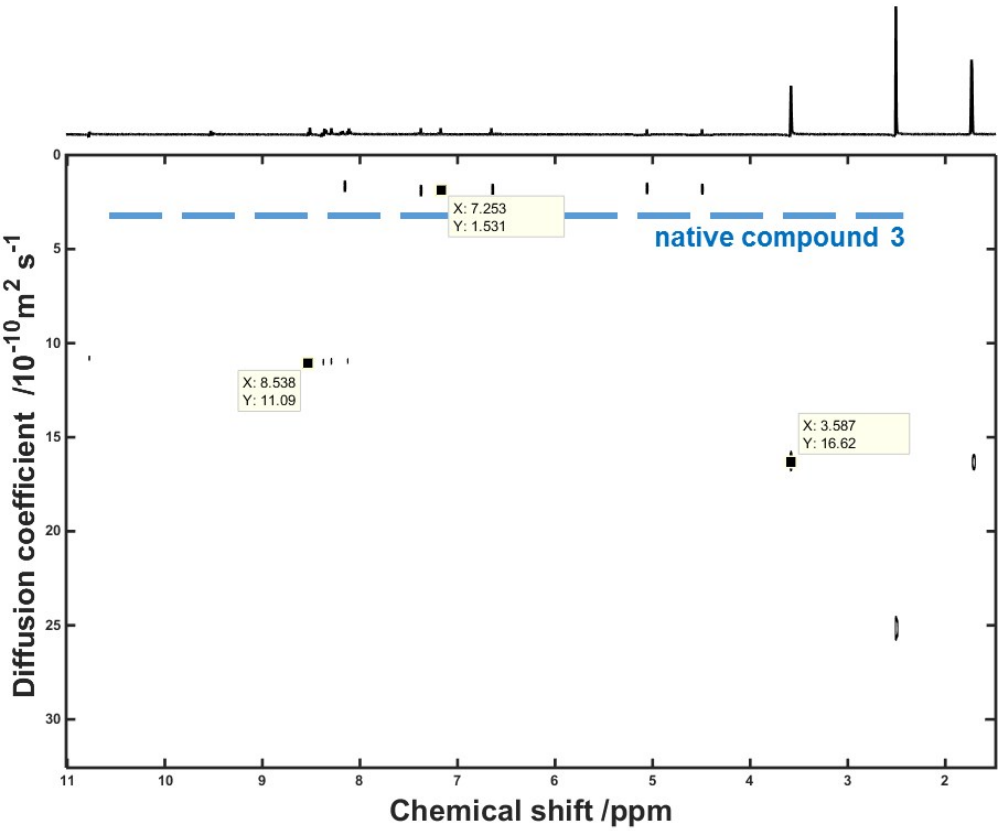

Figure S18. ^{1}H DOSY NMR (THF-d_8, 500 MHz) spectrum of cage **3** with 800 mol% of 1-pyrenecarboxaldehyde (**G-6**) added. The dashed blue line represents the diffusion coefficient value for the native cage **3**.

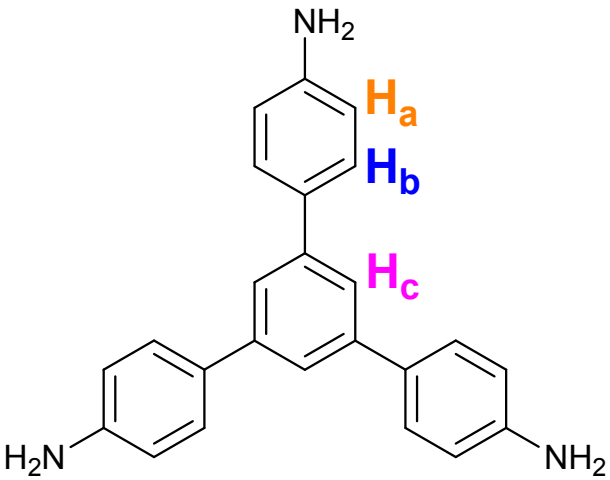

2

Figure S19. Structure of the compound **2** with the atom labels marked.

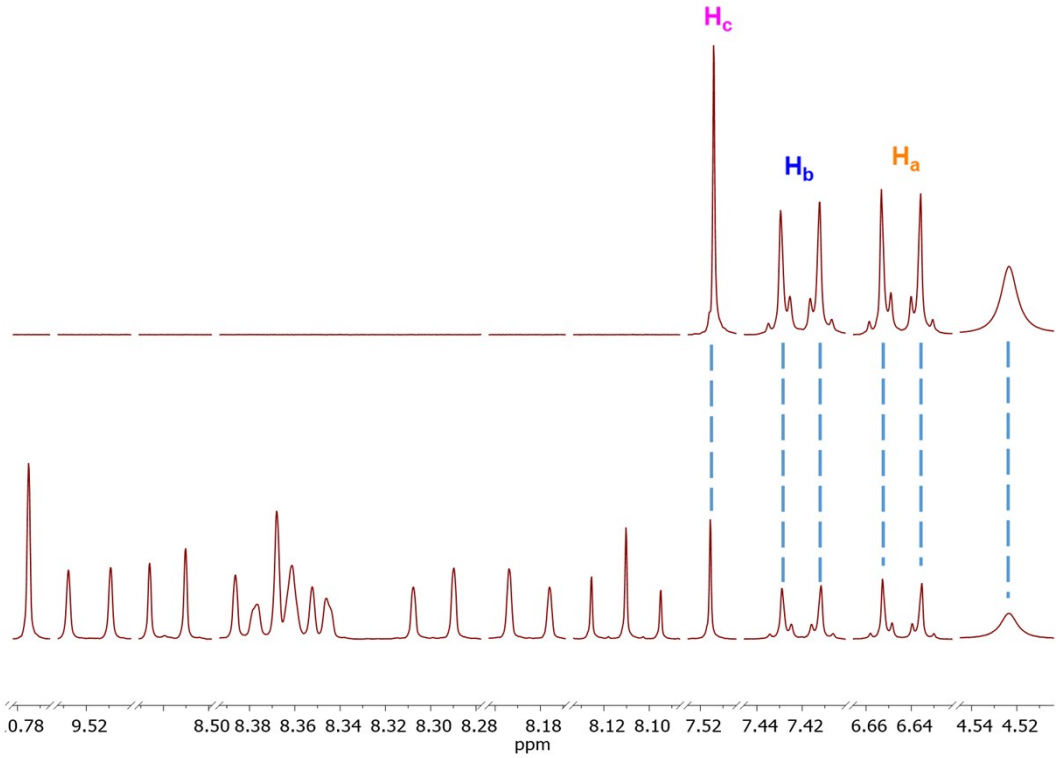

Figure S20. ^{1}H NMR (THF-d_8, 500 MHz) spectrum of compound **2** (**top**) and ^{1}H NMR (THF-d_8, 500 MHz) spectrum of compound **2** with 800 mol% of 1-pyrenecarboxaldehyde (**G-6**) added (**bottom**). For the atom labels of compound **2**, see Figure S19.

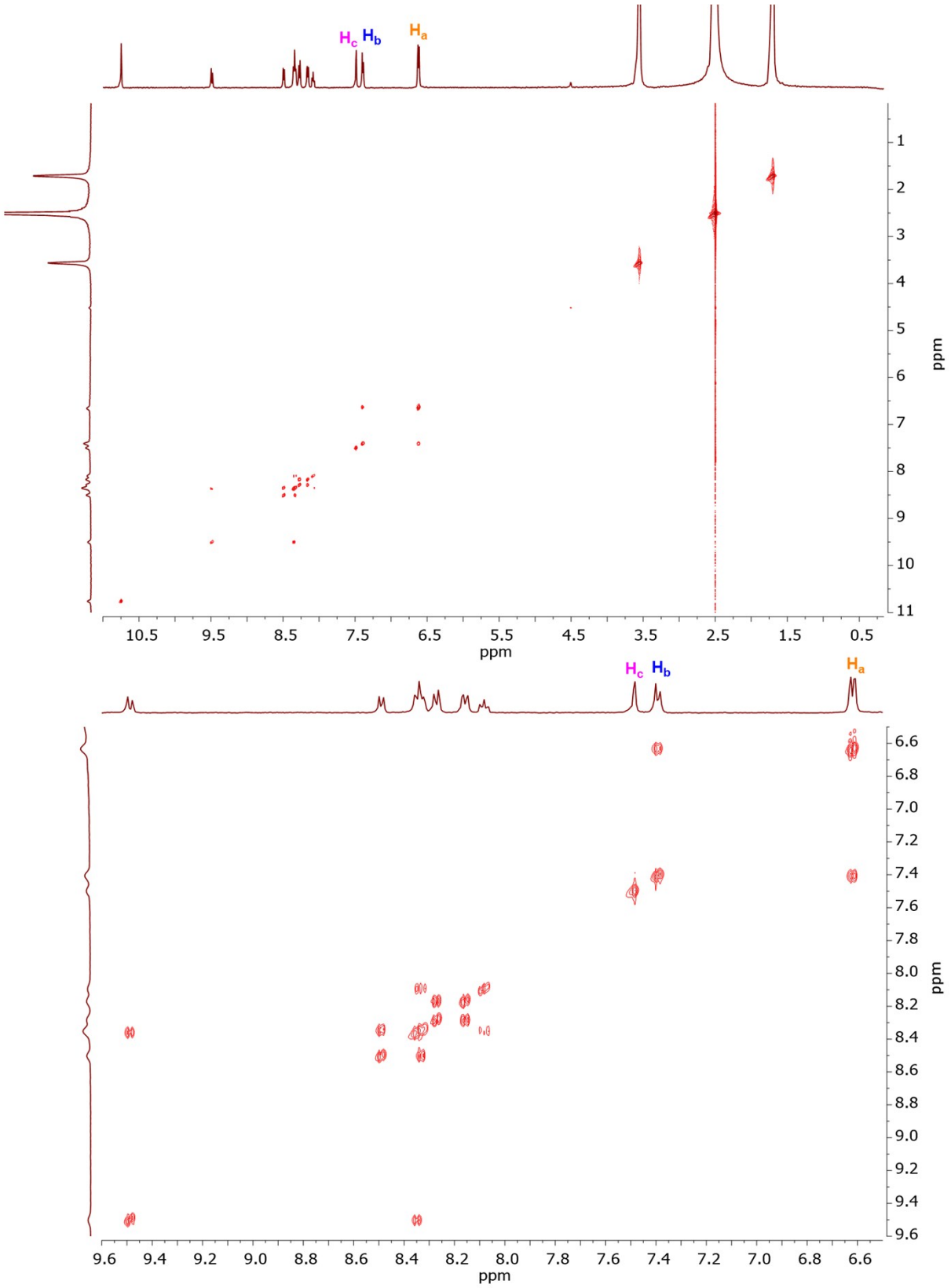

Figure S21. ^{1}H-^{1}H ROESY NMR (THF-d_8, 500 MHz) spectrum of compound **2** with 800 mol% of 1-pyrenecarboxaldehyde (**G-6**) added (**top**) and 9.60-6.50 ppm inset of this spectrum (**bottom**). For the atom labels of compound **2**, see Figure S19.

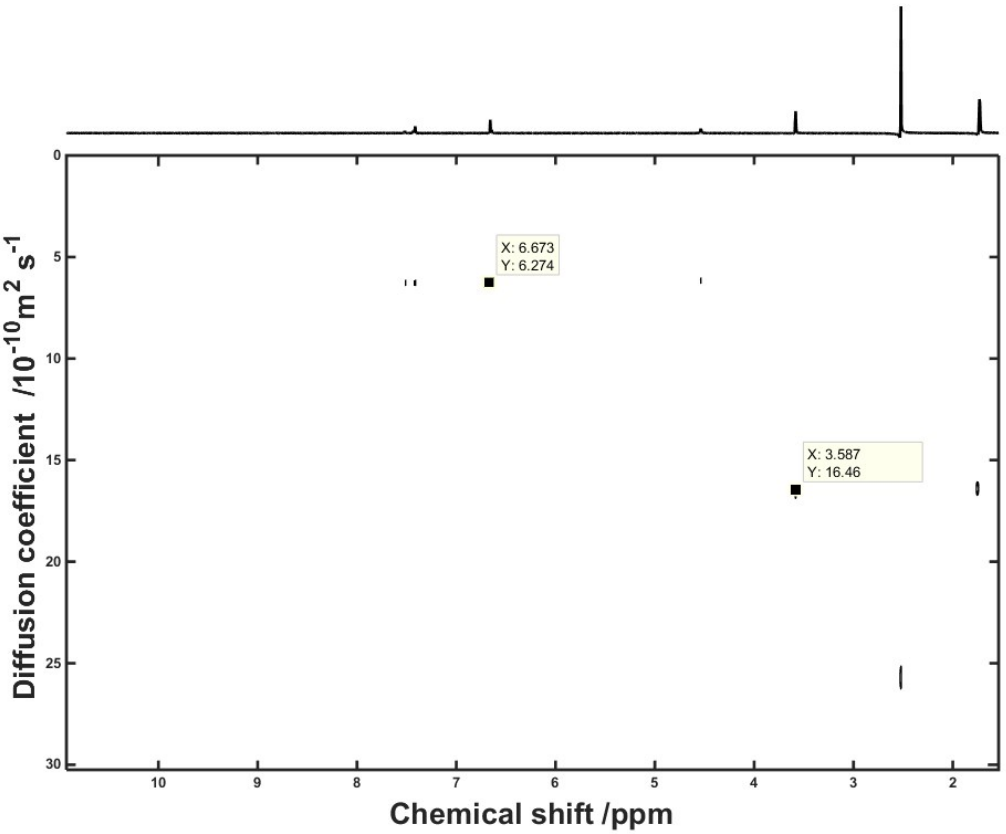

Figure S22. ^{1}H DOSY NMR (THF-d_8, 500 MHz) spectrum of compound **2**.

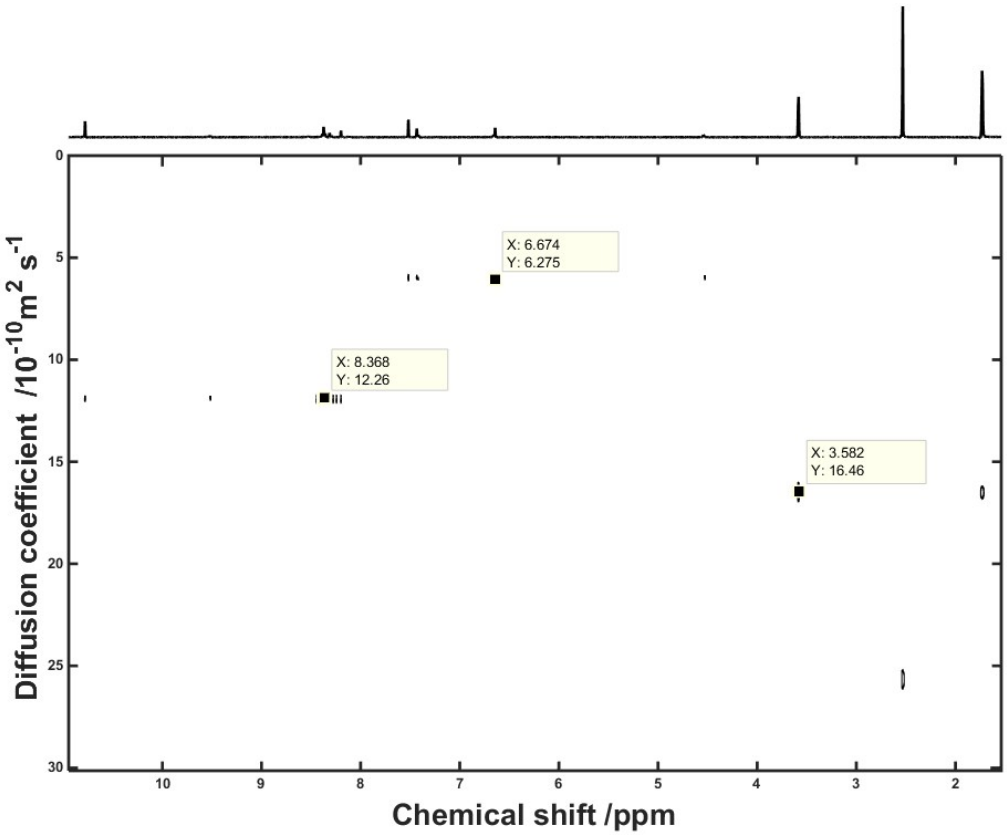

Figure S23. ^{1}H DOSY NMR (THF-d_8, 500 MHz) spectrum of compound **2** with 800 mol% of 1-pyrenecarboxaldehyde (**G-6**) added.

S7. Synthesis of 1,1′-biphenyls – ^{1}H NMR spectra

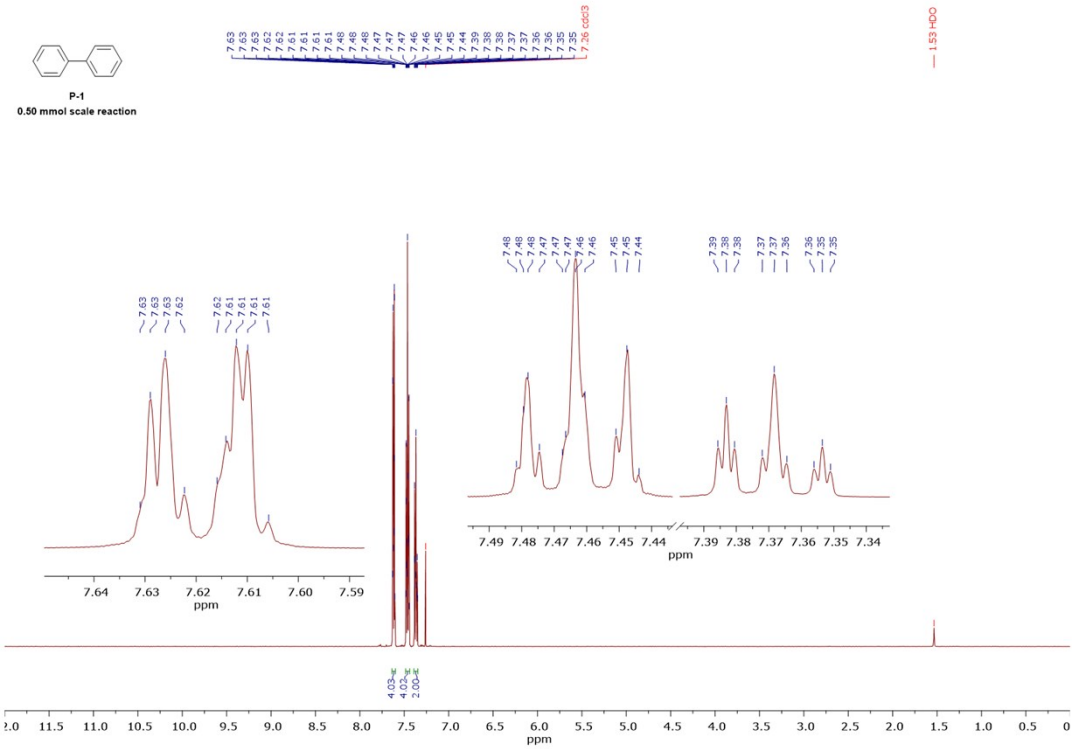

Figure S24. ^{1}H NMR ($CDCl_3$, 500 MHz) spectrum of 1,1′-biphenyl (**P-1**) obtained in a 0.50 mmol scale reaction.

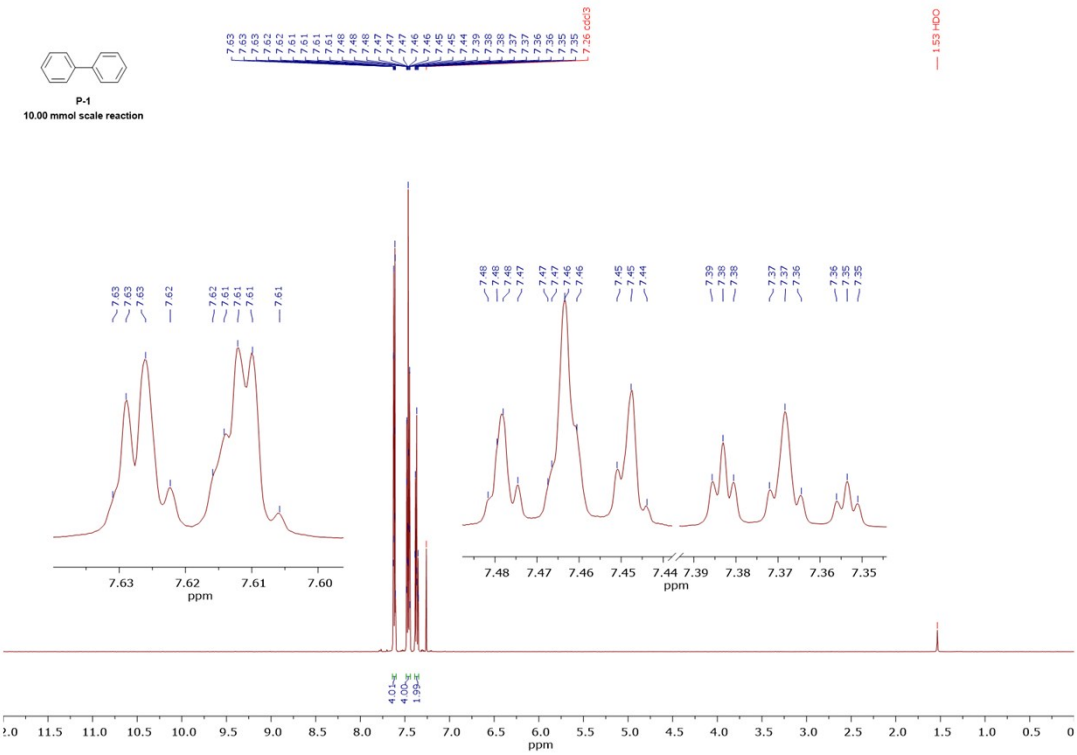

Figure S25. ^{1}H NMR ($CDCl_3$, 500 MHz) spectrum of 1,1′-biphenyl (**P-1**) obtained in a 10.00 mmol scale reaction.

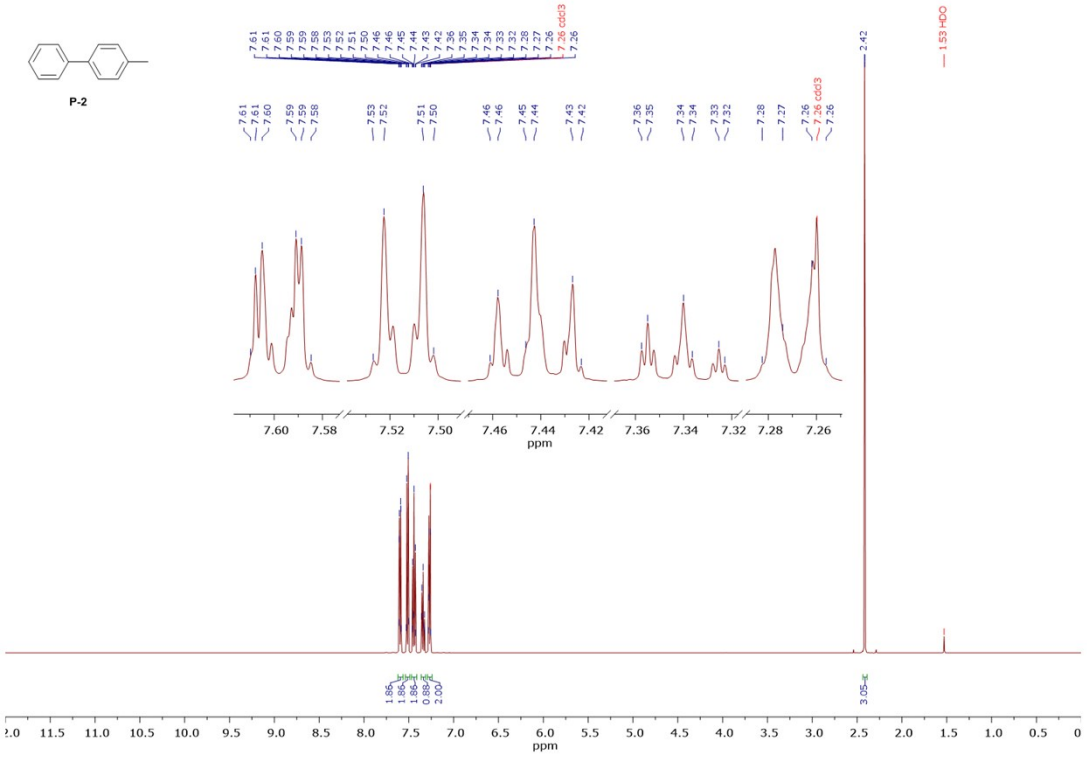

Figure S26. ^{1}H NMR ($CDCl_3$, 500 MHz) spectrum of 4-methyl-1,1′-biphenyl (**P-2**).

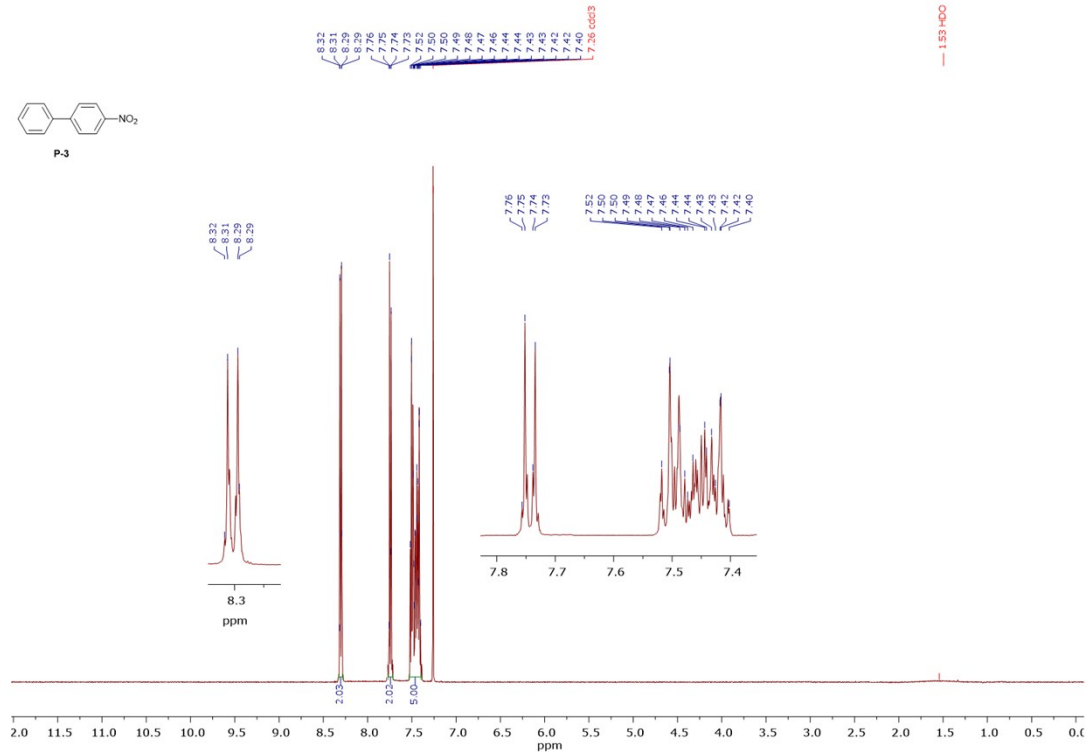

Figure S27. ^{1}H NMR ($CDCl_3$, 500 MHz) spectrum of 4-nitro-1,1′-biphenyl (**P-3**).

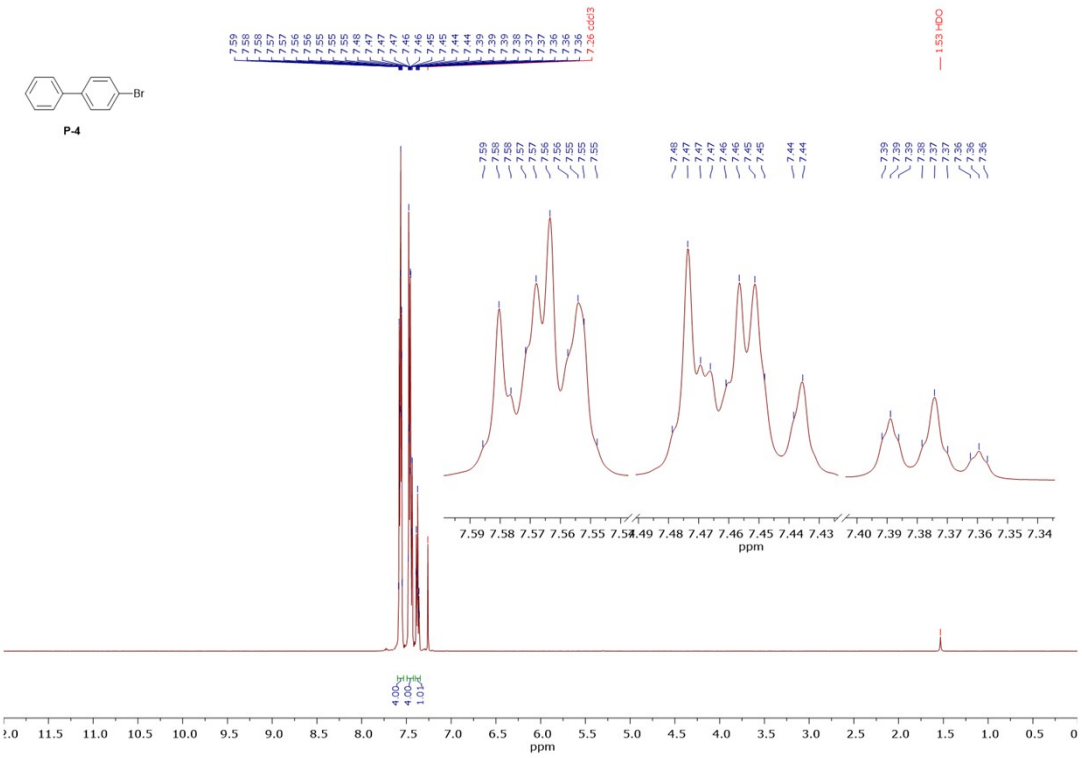

Figure S28. ^{1}H NMR ($CDCl_3$, 500 MHz) spectrum of 4-bromo-1,1′-biphenyl (**P-4**).

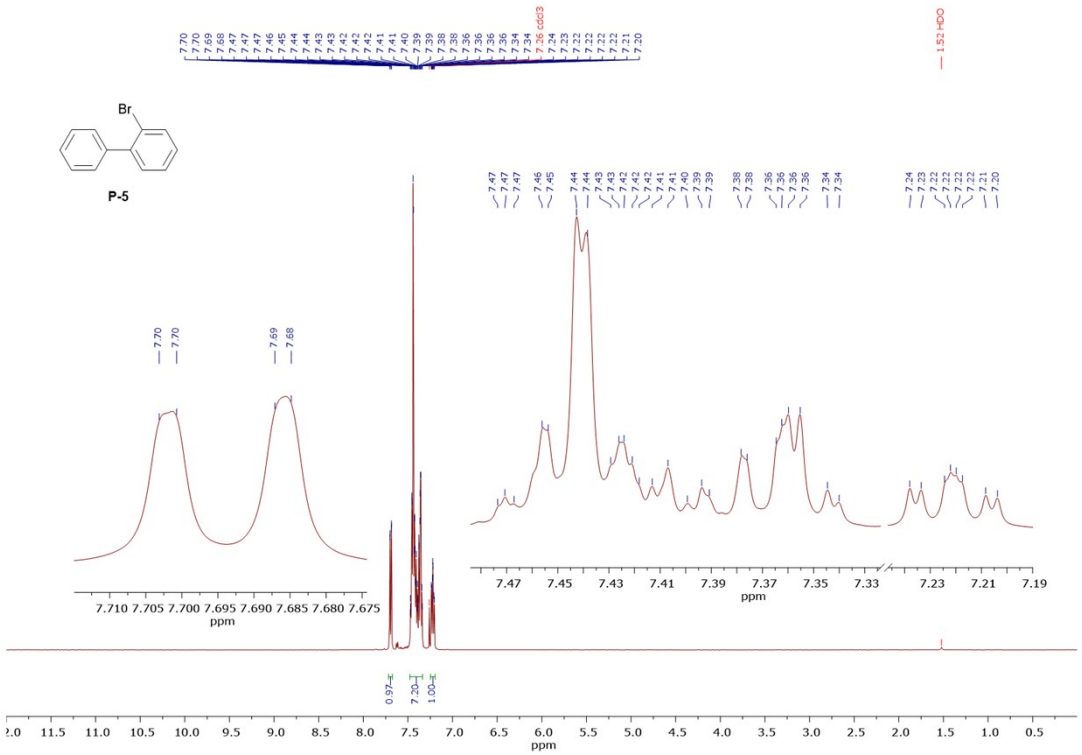

Figure S29. ^{1}H NMR ($CDCl_3$, 500 MHz) spectrum of 2-bromo-1,1′-biphenyl (**P-5**).

S8. Recyclability studies

a)

b)

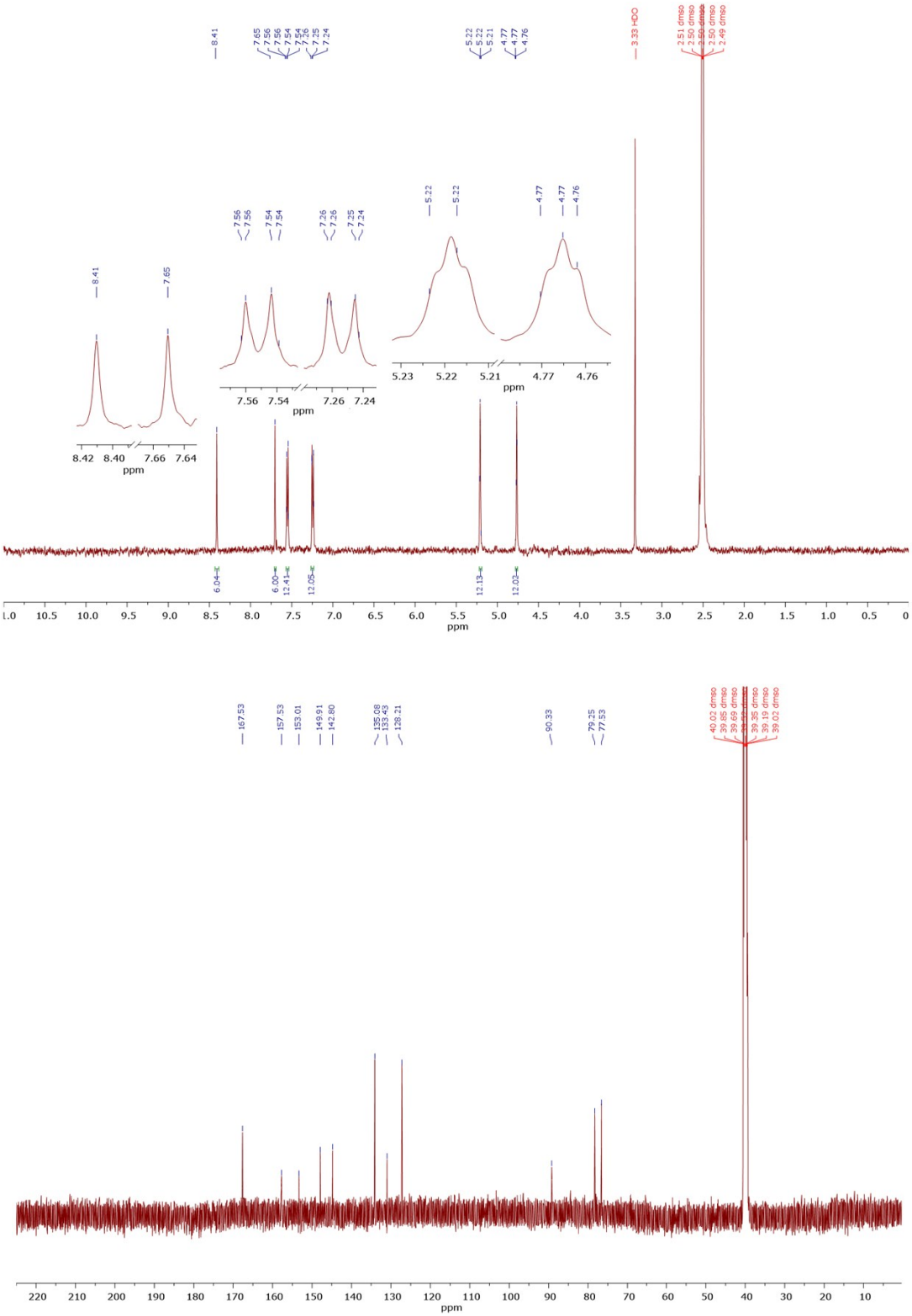

Figure S30. (**a**) ^{1}H NMR (DMSO-d_6, 500 MHz) and (**b**) ^{13}C NMR (DMSO-d_6, 125 MHz) spectra of a catalyst recovered after the catalytic reaction.

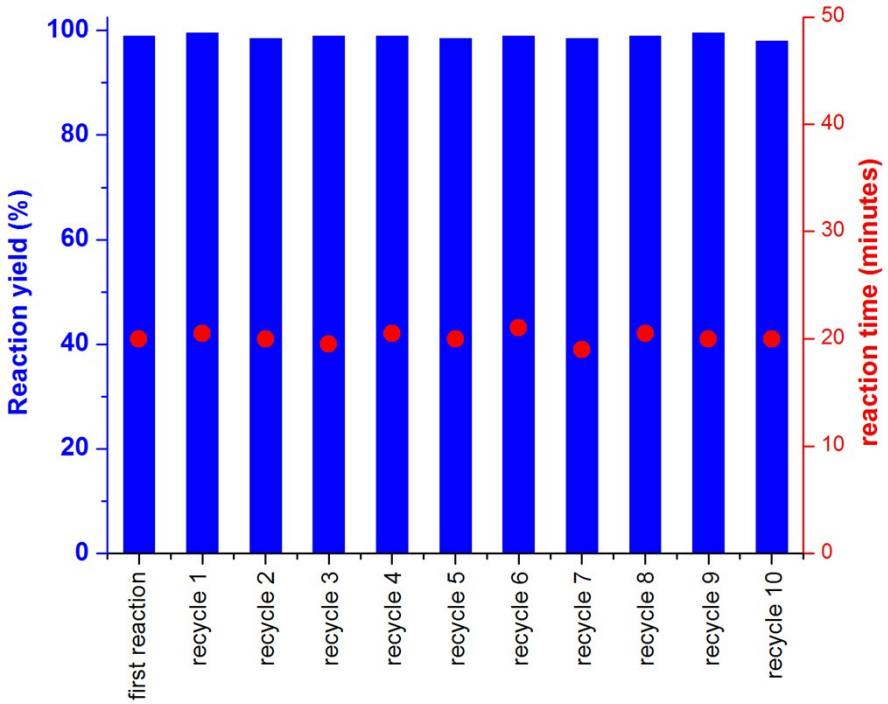

Figure S31. Reusability studies.

S9. UV-Vis titration, PL titration spectra, Job's plot analyses and calculation of binding parameters for the studied non-covalent systems

At first, the UV-Vis (Figure S32) and PL (Figure S33) titration spectra in THF were measured for cage **3** in the presence of representative **G-1**. Lowering of the absorption or emission intensity for cage **3** was observed after the addition of next portions of the **G-1**. PL titration method was found as the more sensitive technique for tracking the recognition. Then, PL titration spectra were measured for cage **3** in the presence of other aromatics (**G-2**-**G-6**; Figures S34-S38). Once again, the lowering of the emission intensity was observed after adding further portions of an aromatic molecule.

Continuous variation method was employed to estimate the system stoichiometry. The Job's plots related to the interactions between **3** and aromatics were constructed (Figures S39-S44). The system stoichiometry was estimated. Interactions of cage **3** with **G-1** or **G-2** featured system stoichiometry of 1:3, whilst for other aromatics (**G-3**-**G-6**) estimated stoichiometry was 1:1.

Calculations of the apparent binding constants (K_{app}) were based on the Stern-Volmer equation[15],[16]:

$$\frac{I_0}{I} = 1 + K_{app} \cdot C_{ar}$$

, where C_{ar} is the molar concentration of the aromatic molecule (**G-1** – **G-6**), I_0 and I are the fluorescence intensity of cage **3** in the absence and in the presence of the aromatic molecule, respectively. I_0/I = f(C_{ar}) dependencies were plotted for **G-1**-**G-6** (Figures S45-S50). All these dependencies were found to be linear. Therefore, K_{app} were calculated respectively using the Stern-Volmer method, see references [15] and [16] for details of this methodology.

Gibbs free energy values (free energies; ΔG) were calculated using the following equation:

$$\Delta G = -RT\ln K_{app}$$

, where R stands for the gas constant (8.314 J·K^{-1}·mol^{-1}) and T is the temperature (298.15 K).

The calculated binding parameters (system stoichiometry, K_{app} and ΔG) are summarized in **Table 1** in the main article file.

For the representative aromatic molecule **G-6** (the highest K_{app} among the aromatics tested), the K_{app} and ΔG values evaluated from PL spectra titration method were also compared with the respective values obtained from ^{1}H DOSY NMR experiments. The method for calculation of these parameters employing the ^{1}H DOSY NMR procedure is described in detail elsewhere.[17]-[19] At first, the spectra for native **G-6** and 1:1 (mol:mol) mixture of cage **3** and **G-6**, were acquired (Figures S51-S52, $c_{cage3} = c_{G\text{-}6}$ = 0.5 mM). The diffusion coefficient for the free **G-6** was higher than the respective value for **G-6** in a presence of cage **3**. This feature was ascribed to the recognition feature of cage **3**.[17]-[19] K_{app} (658 M^{-1}) and ΔG (−16.1 kJ·mol^{-1}) values calculated employing the ^{1}H DOSY NMR method were highly consistent with the data obtained from PL experiments, see Table S4.

We would like note that, in general, the Stern-Volmer methodology is used to describe 1:1 models. However, I_0/I = f(C_{ar}) plots were linear for all studied systems.

Therefore, this method was employed to calculate each K_{app}. For additional discussion, see for example: A. Kasprzak, H. Sakurai., *Dalton Trans*. **2019**, *48*, 17147;

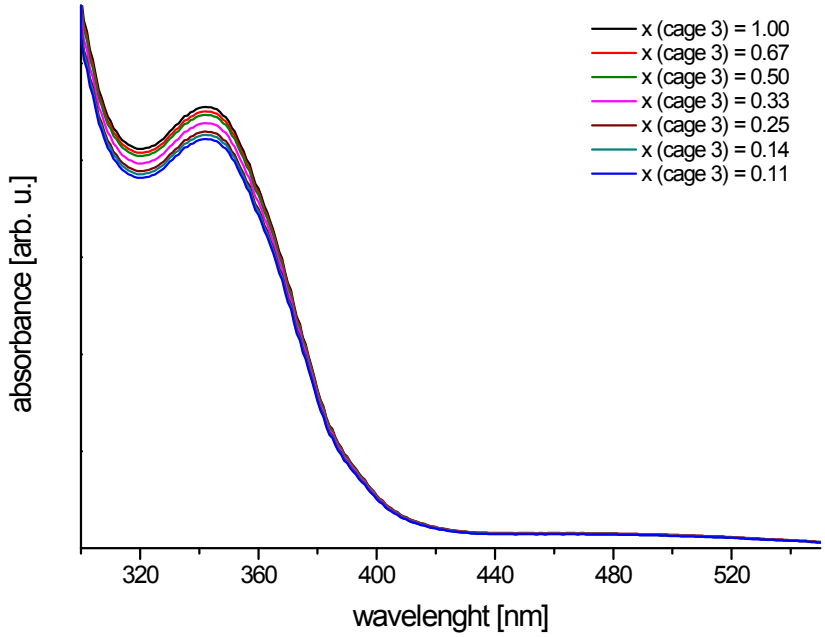

Figure S32. UV-Vis titration spectra of cage **3** in the presence of further portions of **G-1** (x stands for the molar fraction of **3**).

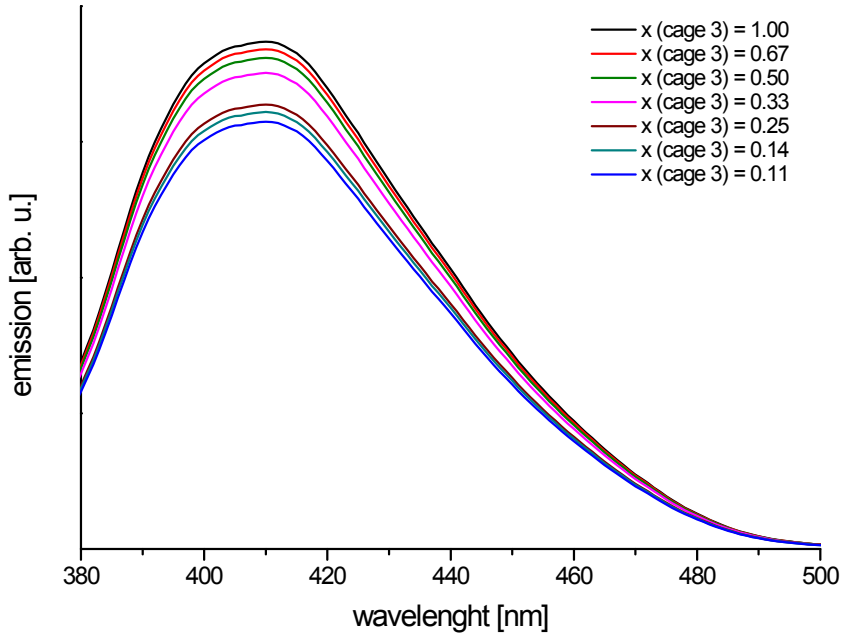

Figure S33. PL titration spectra of cage **3** in the presence of further portions of **G-1** (excitation wavelength: 335 nm; x stands for the molar fraction of **3**).

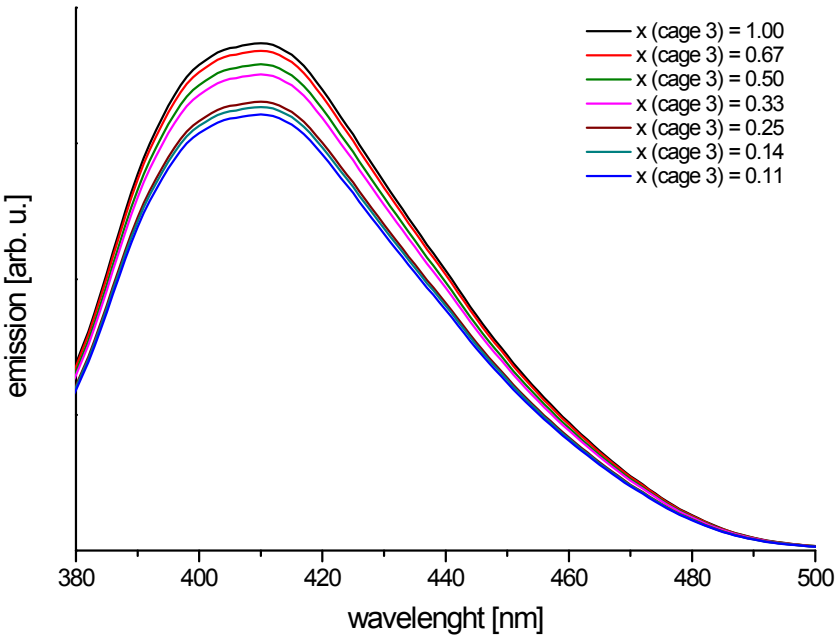

Figure S34. PL titration spectra of cage **3** in the presence of further portions of **G-2** (excitation wavelength: 335 nm; x stands for the molar fraction of **3**).

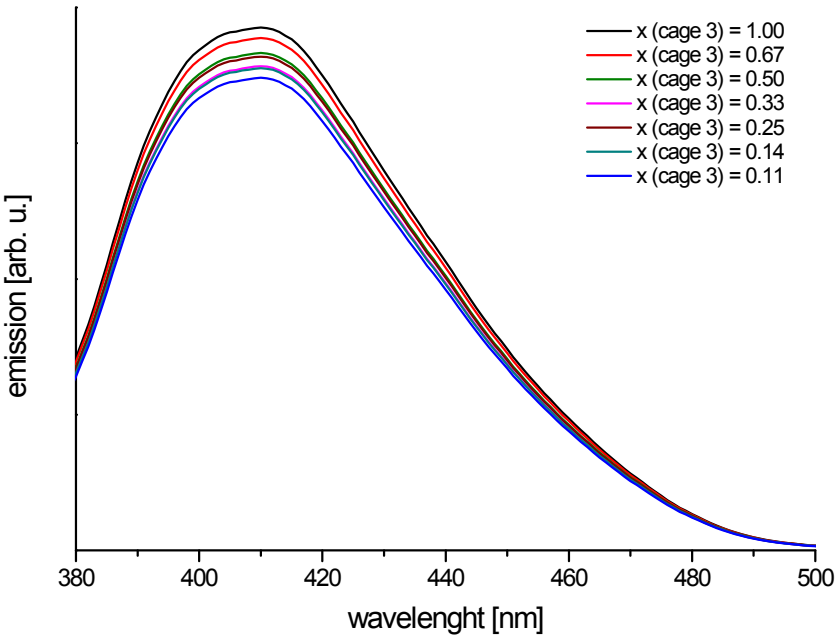

Figure S35. PL titration spectra of cage **3** in the presence of further portions of **G-3** (excitation wavelength: 335 nm; x stands for the molar fraction of **3**).

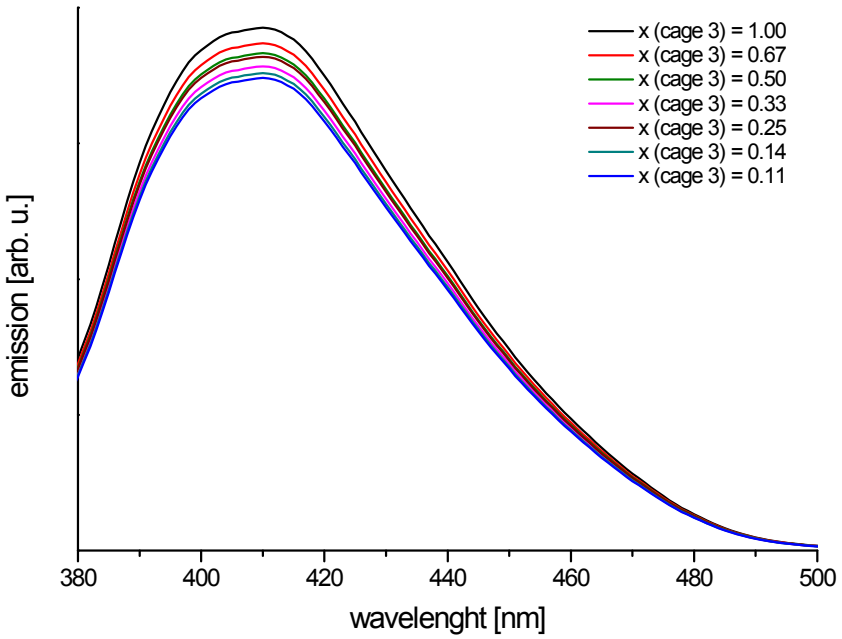

Figure S36. PL titration spectra of cage **3** in the presence of further portions of **G-4** (excitation wavelength: 335 nm; x stands for the molar fraction of **3**).

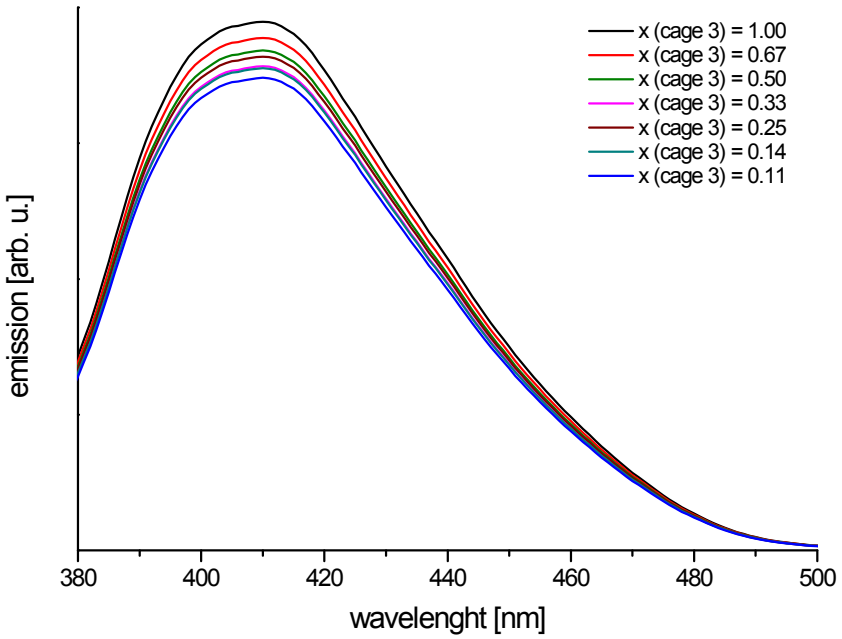

Figure S37. PL titration spectra of cage **3** in the presence of further portions of **G-5** (excitation wavelength: 335 nm; x stands for the molar fraction of **3**).

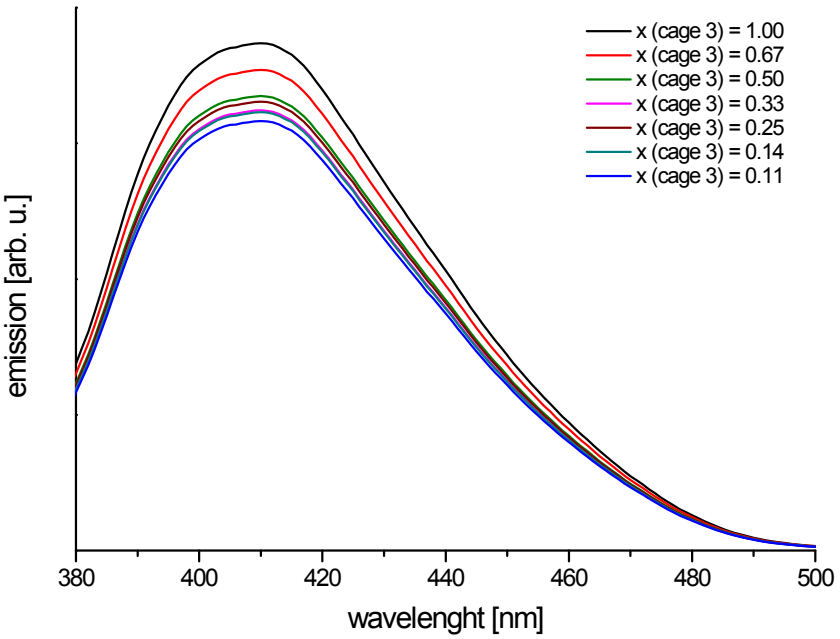

Figure S38. PL titration spectra of cage **3** in the presence of further portions of **G-6** (excitation wavelength: 335 nm; x stands for the molar fraction of **3**).

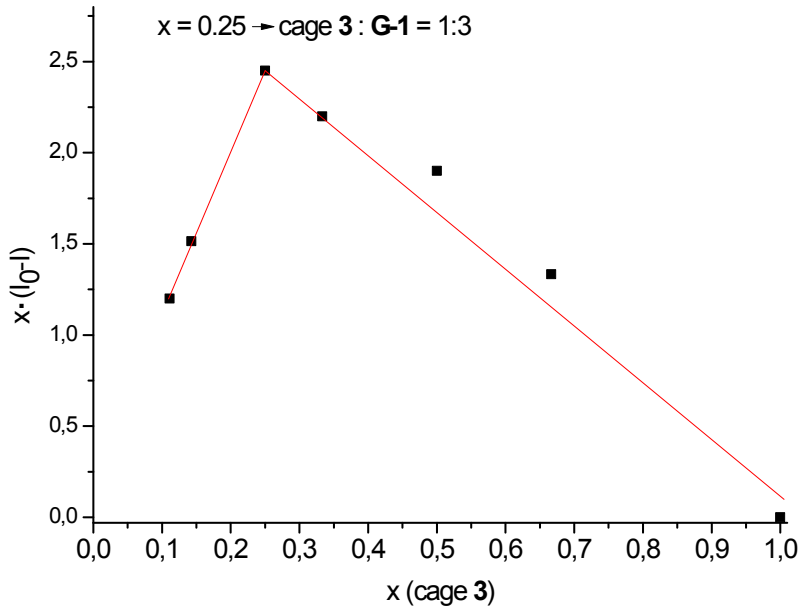

Figure S39. Job's plot regarding the interactions between cage **3** and **G-1** (obtained from the PL spectra titration data; x stands for the molar fraction of **3**, I_0 stands for the emission intensity of **3** without aromatic molecule added, I stands for the emission intensity of **3** with the given amount of aromatic molecule added).

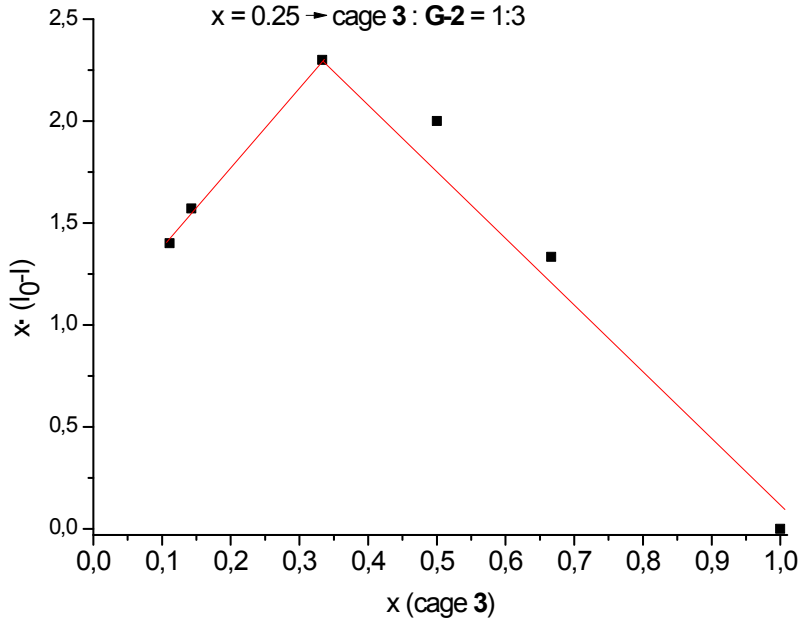

Figure S40. Job's plot regarding the interactions between cage **3** and **G-2**. (obtained from the PL spectra titration data; x stands for the molar fraction of **3**, I_0 stands for the emission intensity of **3** without aromatic molecule added, I stands for the emission intensity of **3** with the given amount of aromatic molecule added).

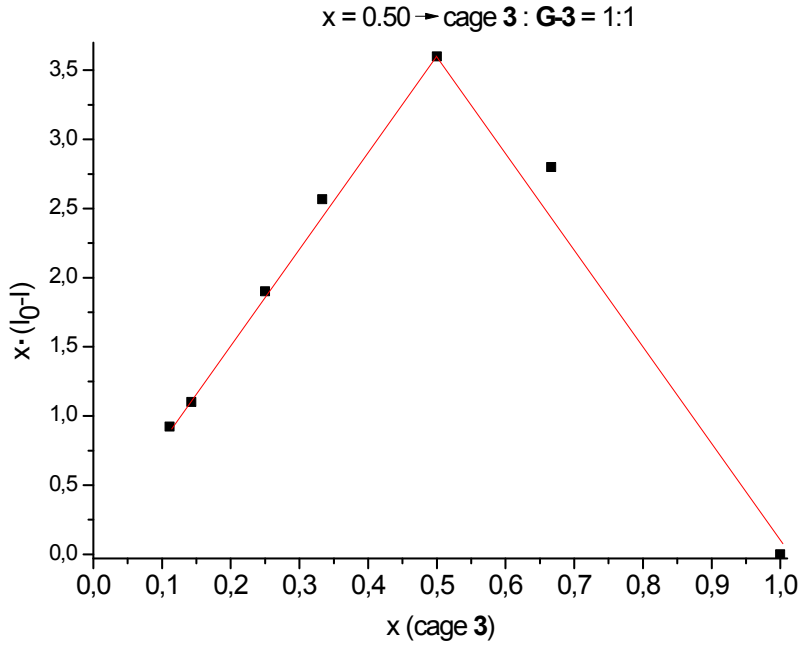

Figure S41. Job's plot regarding the interactions between cage **3** and **G-3**. (obtained from the PL spectra titration data; x stands for the molar fraction of **3**, I_0 stands for the emission intensity of **3** without aromatic molecule added, I stands for the emission intensity of **3** with the given amount of aromatic molecule added).

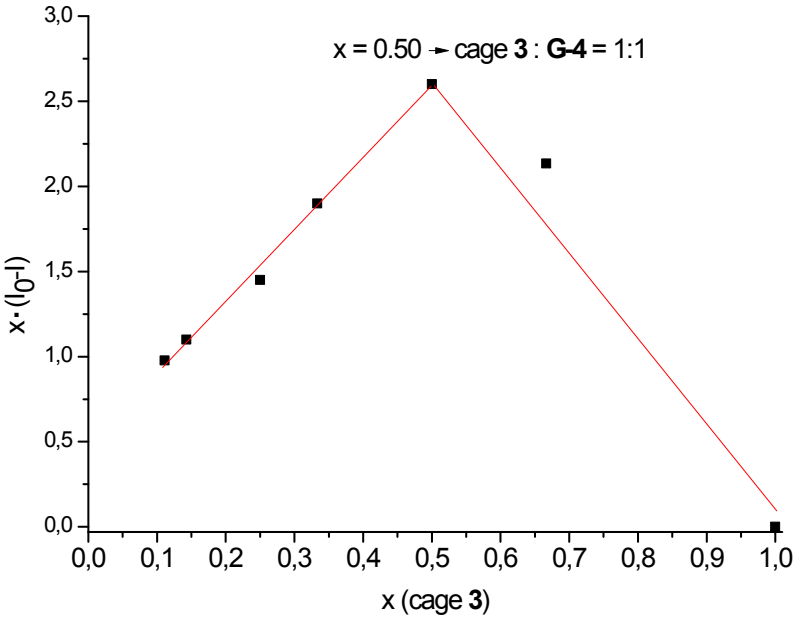

Figure S42. Job's plot regarding the interactions between cage **3** and **G-4**. (obtained from the PL spectra titration data; x stands for the molar fraction of **3**, I_0 stands for the emission intensity of **3** without aromatic molecule added, I stands for the emission intensity of **3** with the given amount of aromatic molecule added).

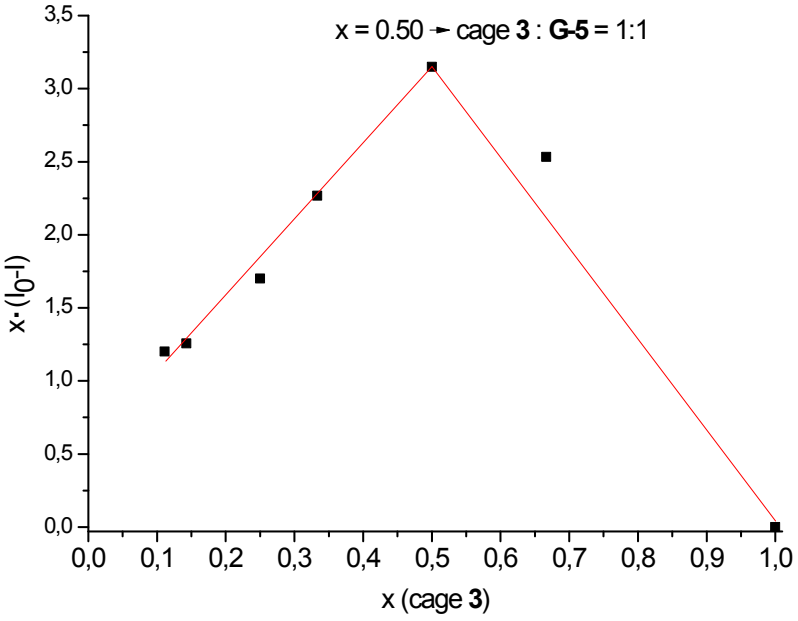

Figure S43. Job's plot regarding the interactions between cage **3** and **G-5**. (obtained from the PL spectra titration data; x stands for the molar fraction of **3**, I_0 stands for the emission intensity of **3** without aromatic molecule added, I stands for the emission intensity of **3** with the given amount of aromatic molecule added).

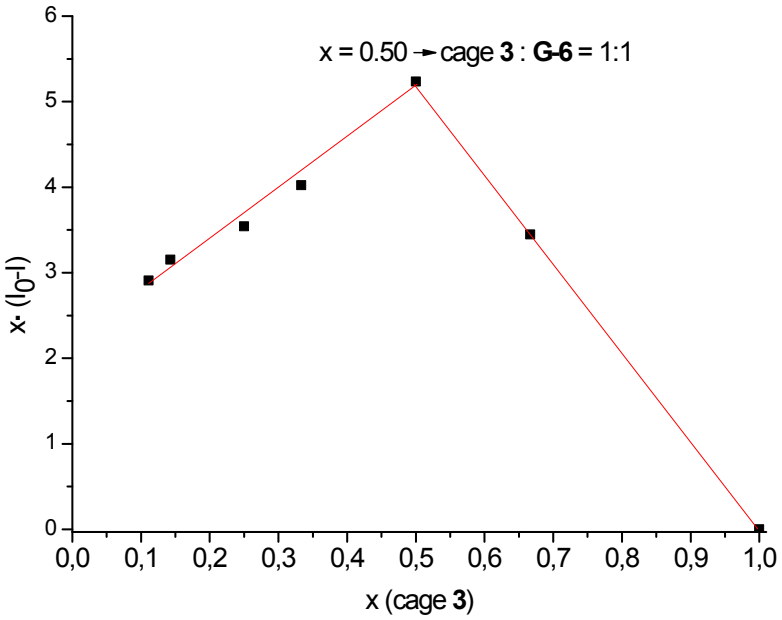

Figure S44. Job's plot regarding the interactions between cage **3** and **G-6**. (obtained from the PL spectra titration data; x stands for the molar fraction of **3**, I_0 stands for the emission intensity of **3** without aromatic molecule added, I stands for the emission intensity of **3** with the given amount of aromatic molecule added)

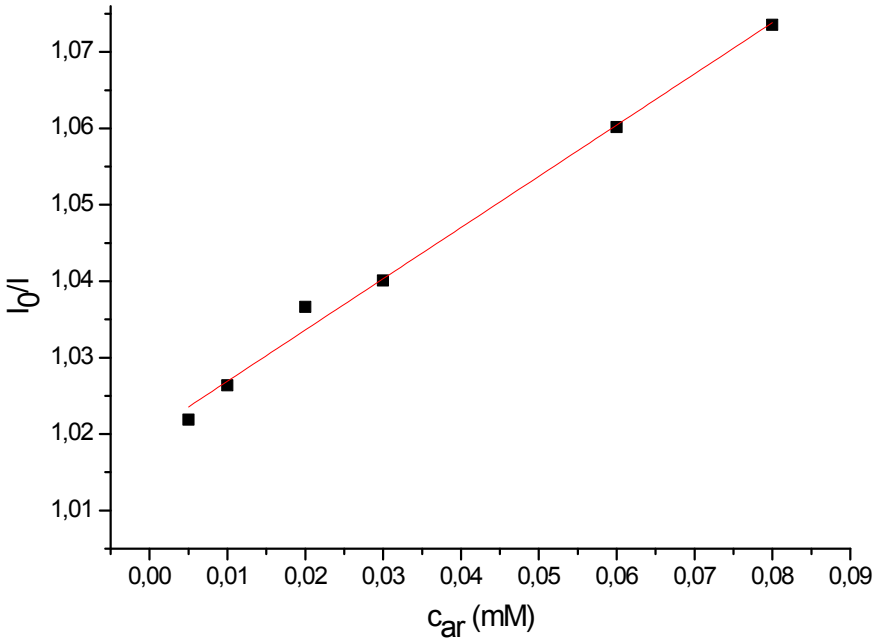

Figure S45. I_0/I = f(C_{ar}) plot regarding the interactions between **3** and **G-1**. R^2 = 0.9923.

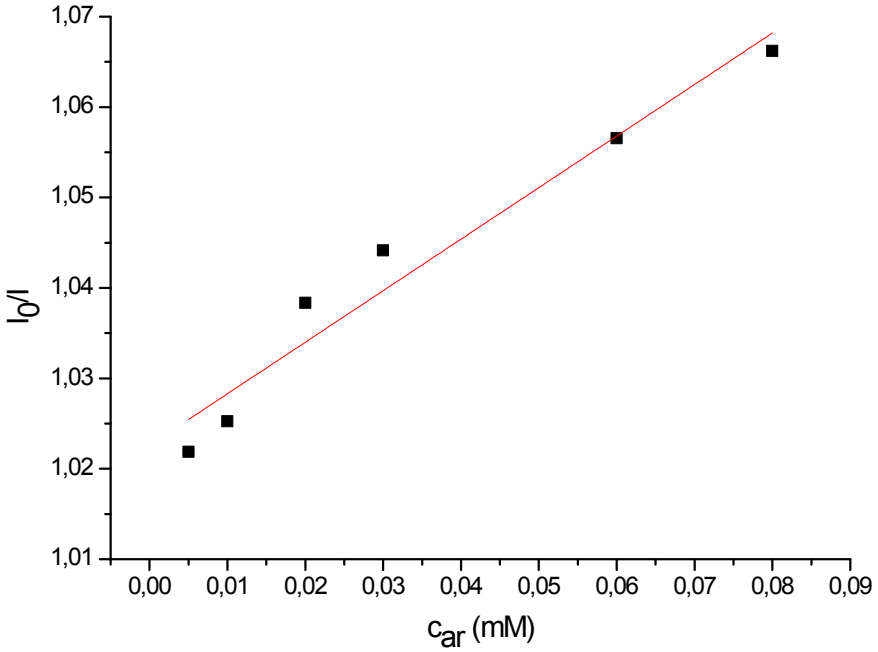

Figure S46. I_0/I = f(C_{ar}) plot regarding the interactions between **3** and **G-2**. R^2 = 0.9650.

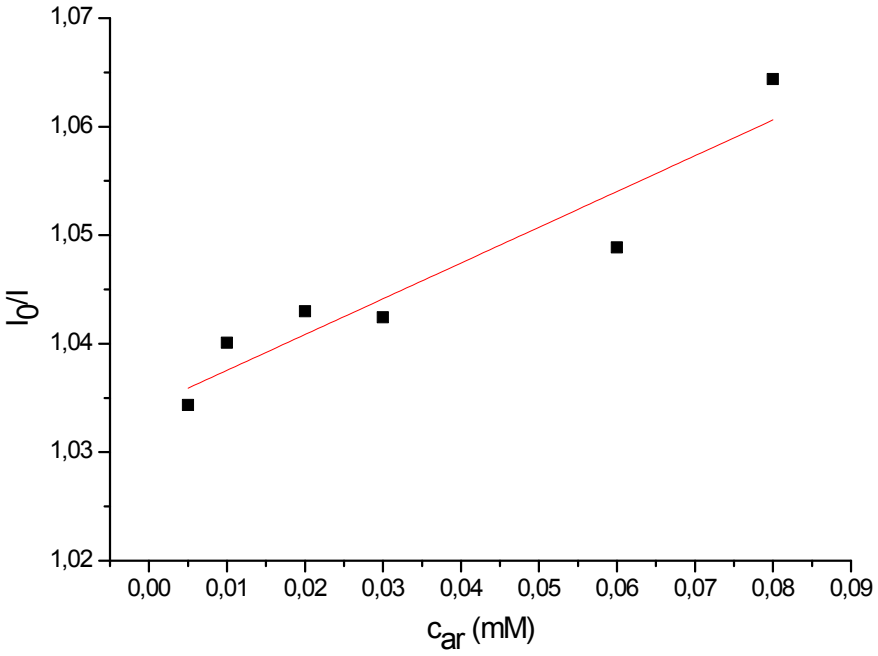

Figure S47. I_0/I = f(C_{ar}) plot regarding the interactions between **3** and **G-3**. R^2 = 0.9052.

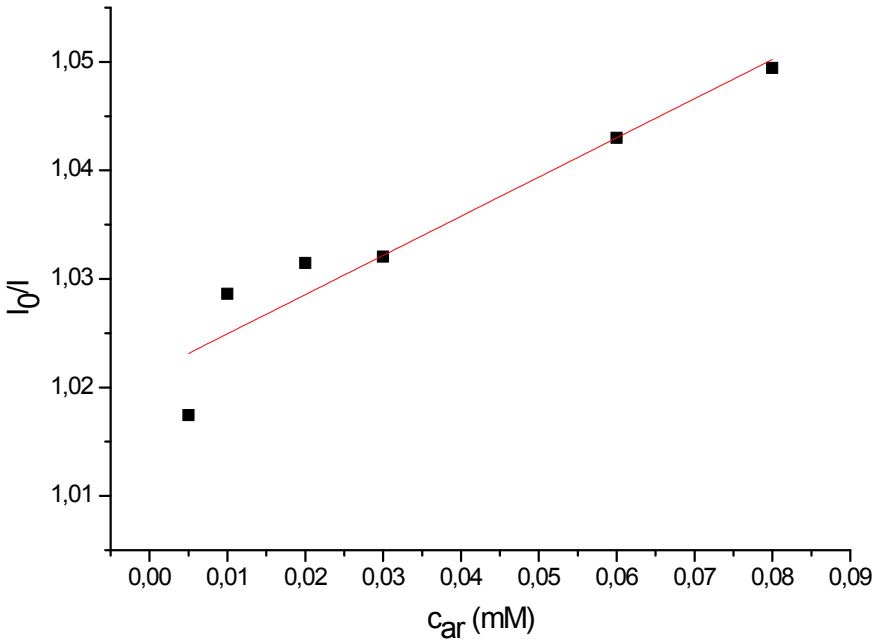

Figure S48. I_0/I = f(C_{ar}) plot regarding the interactions between **3** and **G-4**. R^2 = 0.9006.

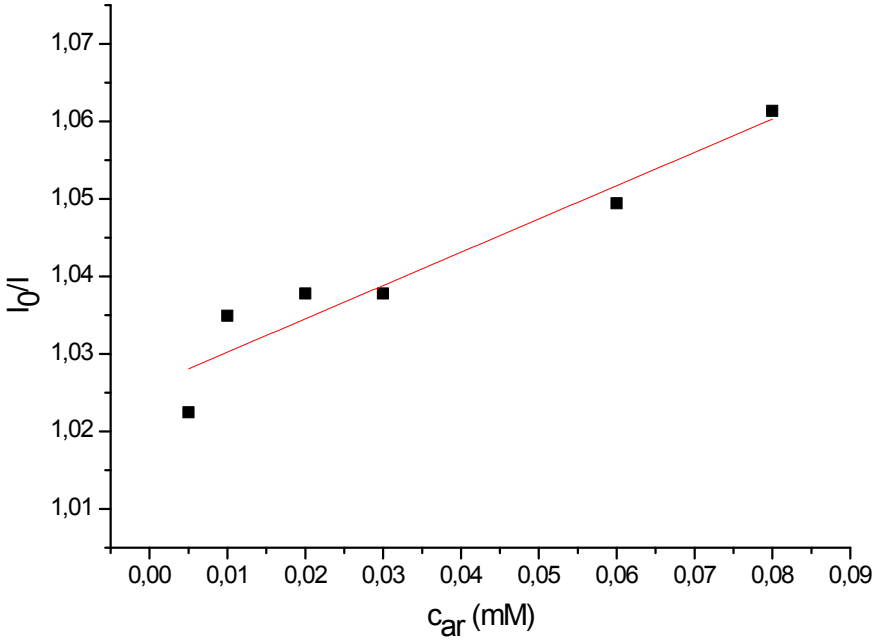

Figure S49. I_0/I = f(C_{ar}) plot regarding the interactions between **3** and **G-5**. R^2 = 0.9015.

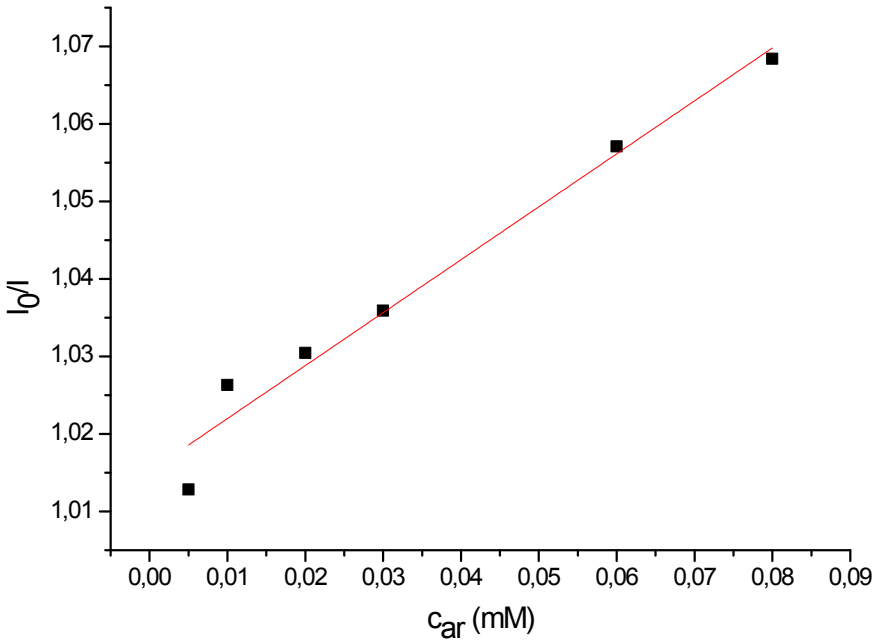

Figure S50. I_0/I = f(C_{ar}) plot regarding the interactions between **3** and **G-6**. R^2 = 0.9663.

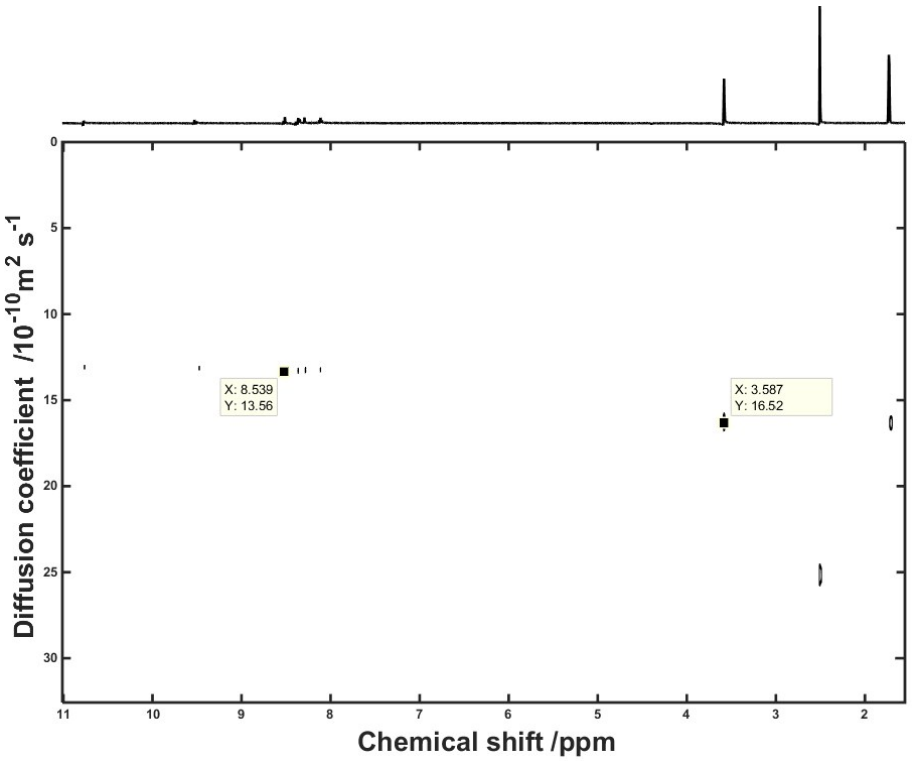

Figure S51. ^{1}H DOSY NMR (THF-d_8, 500 MHz) spectrum of native **G-6**.

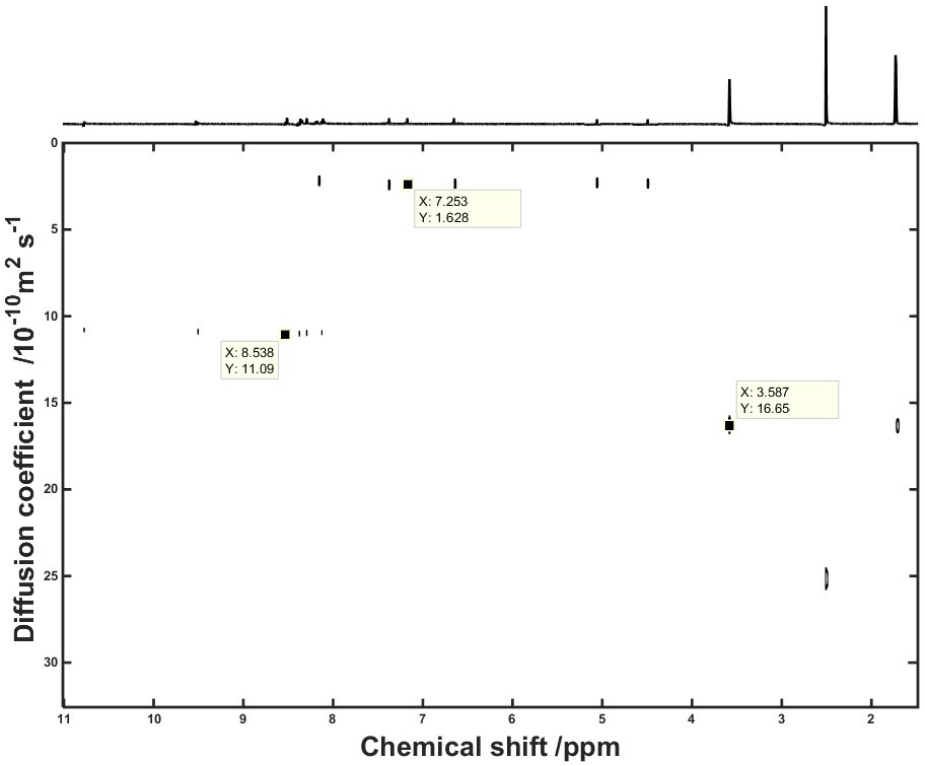

Figure S52. ^{1}H DOSY NMR (THF-d_8, 500 MHz) spectrum of 1:1 (mol:mol) mixture of cage **3** and **G-6**.

Table S4. K_{app} and ΔG values for the interactions between cage **3** and **G-6** calculated from ^{1}H DOSY NMR data. Diffusion coefficient values are given in 10^{-10} m^2 s^{-1}; x_b parameter was calculated as follows: $x_b = (D_{free} - D_{obs}) \cdot [(D_{free} - D_{bound})^{-1}]$, where D_{free} stands for the diffusion coefficient value for the native **G-6**, D_{obs} is the diffusion coefficient value for the **G-6** in the system, D_{bound} is the diffusion coefficient value for cage **3** in the system; K_{app} values were calculated as follows: $K_{app} = x_b \cdot [(1 - x_b) \cdot (0.5\ mM - x_b \cdot 0.5\ mM)]^{-1}$. The respective K_{app} and ΔG values evaluated from PL titration experiments are also shown.

Component	D_{free}	D_{obs}	D_{bound}	x_b	K_{app} /M^{-1} (K_{app} value calculated based on PL experiments data)	ΔG /kJ·mol^{-1} (ΔG value calculated based on PL experiments data)
Cage **3**	N/A	N/A	1.628	0.207	**658**	**−16.1**
G-6	13.560	11.090	N/A		(650)	(−16.1)

S10. Kinetic studies

^{1}H NMR spectra were measured in DMSO-d_6 in time intervals (2 minutes, 5 minutes, 10 minutes, 15 minutes and 20 minutes). Phenylboronic acid (**G-1**) and chlorobenzene (**G-2**) were used as the reactants. The reactions monitored by ^{1}H NMR were conducted on the basis of the designed general procedure for the synthesis of 1,1′-biphenyls presented in Section S1.6, ESI. The spectra were measured (i) in the absence of the catalyst (Figure S53), (ii) in the presence of 0.5 mol% of the cage **5** as the catalyst (Figure S54), or (iii) in the presence of cage **5** (0.5 mol%) as catalyst and **G-6** (100 mol%) as the competing aromatic molecule (Figure S55). Kinetic curves constructed based on the Michaelis-Menten model and the respective Lineweaver-Burk plots are presented in Figures S56-S57. For the details of this methodology, see for example reference [20].

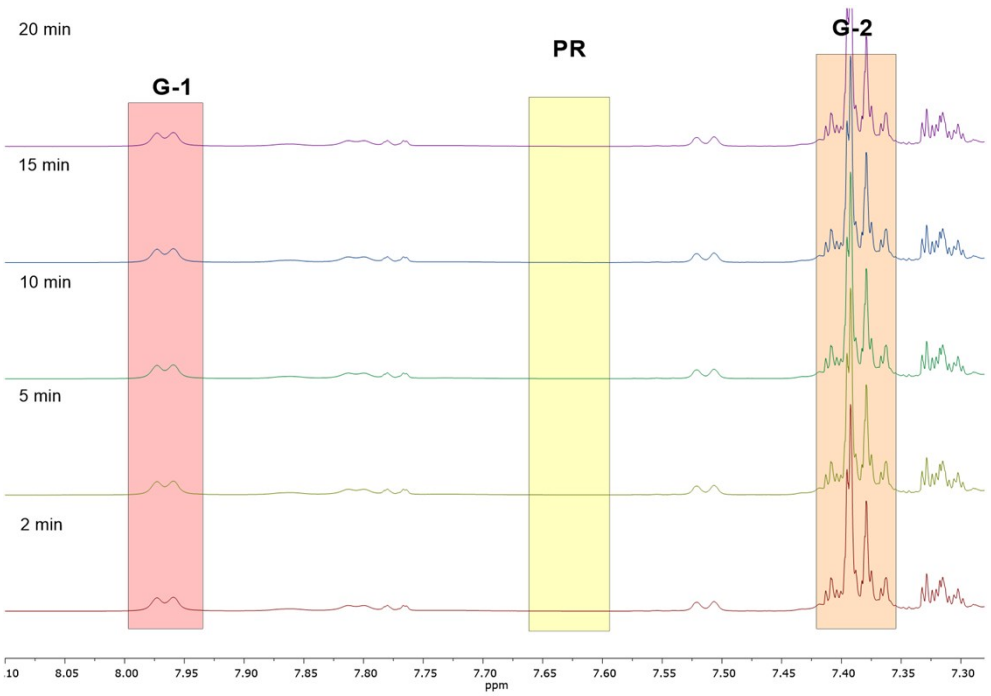

Figure S53. Evolution of ^{1}H NMR spectra during the reaction between phenylboronic acid (**G-1**) and chlorobenzene (**G-2**) without catalyst added. **PR** = product (1,1′-biphenyl). The crucial inset of the spectra is presented. The representative signals' locations for **G-1**, **G-2** and **PR** are marked with colours.

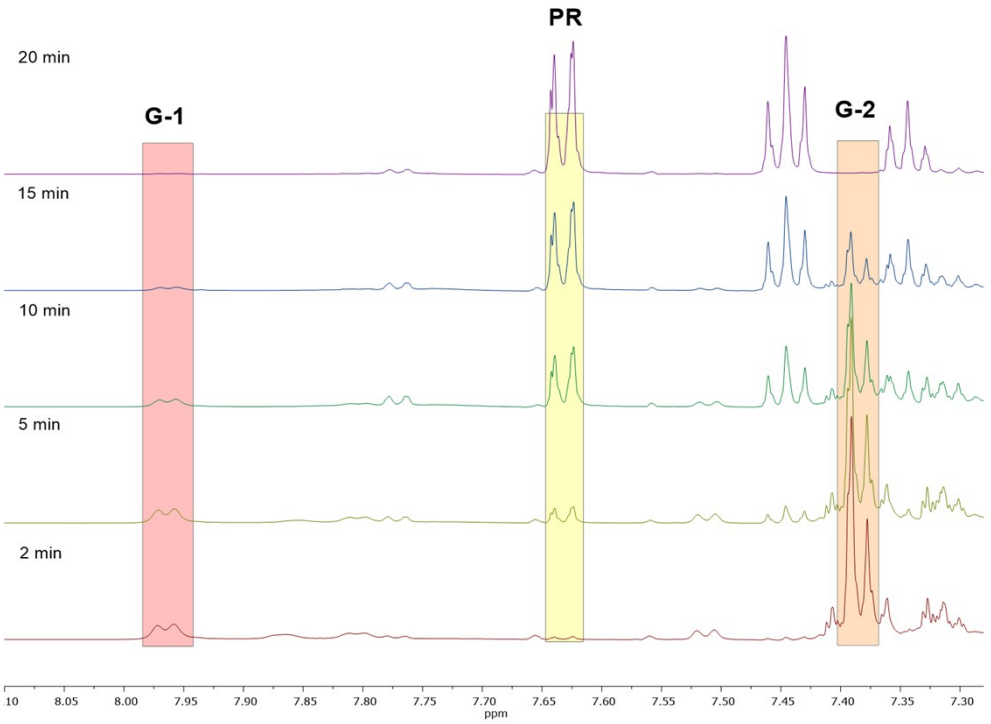

Figure S54. Evolution of ^{1}H NMR spectra during the reaction between phenylboronic acid (**G-1**) and chlorobenzene (**G-2**) in the presence of cage **5** (0.5 mol%) as catalyst. **PR** = product (1,1′-biphenyl). The crucial inset of the spectra is presented. The representative signals' locations for **G-1**, **G-2** and **PR** are marked with colours.

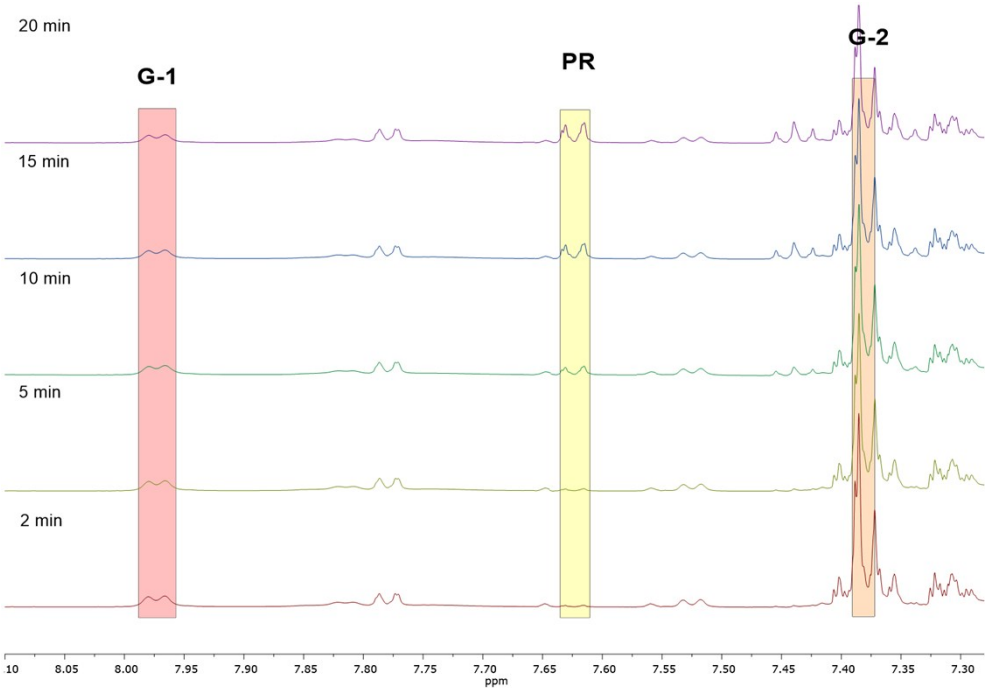

Figure S55. Evolution of ^{1}H NMR spectra during the reaction between phenylboronic acid (**G-1**) and chlorobenzene (**G-2**) in the presence of cage **5** (0.5 mol%) as catalyst and 1-pyrenecarboxaldehyde (**G-6**) as the competing aromatic molecule. **PR** = product (1,1′-biphenyl). The crucial inset of the spectra is presented. The representative signals' locations for **G-1**, **G-2** and **PR** are marked with colours.

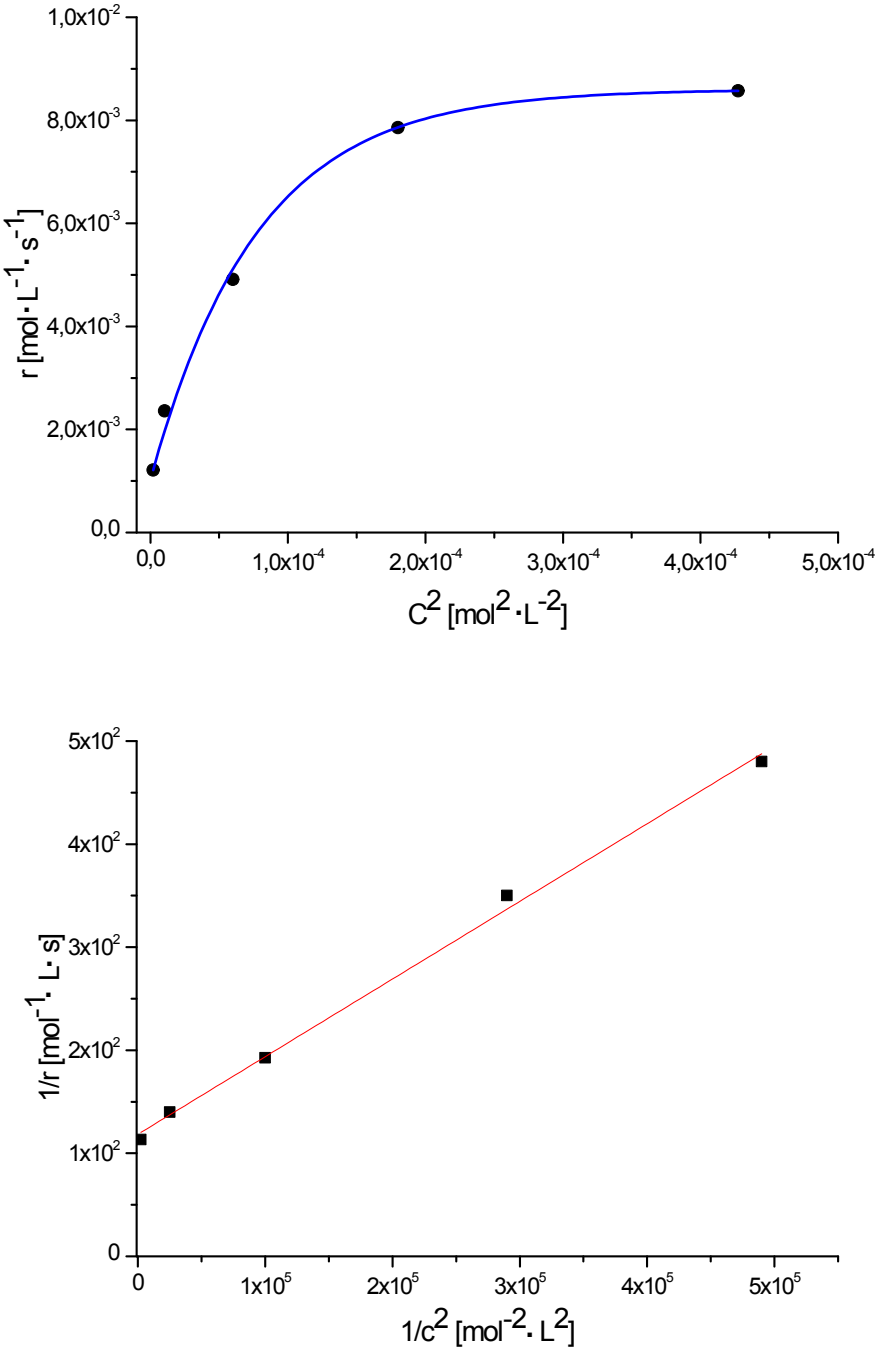

Figure S56. Kinetic plot constructed based on the Michaelis-Menten model (**top**) and the respective Lineweaver-Burk plot (**bottom**) for the reaction in the presence of cage **5** (0.5 mol%) as catalyst (Figure S53), R^2 = 0.9961.

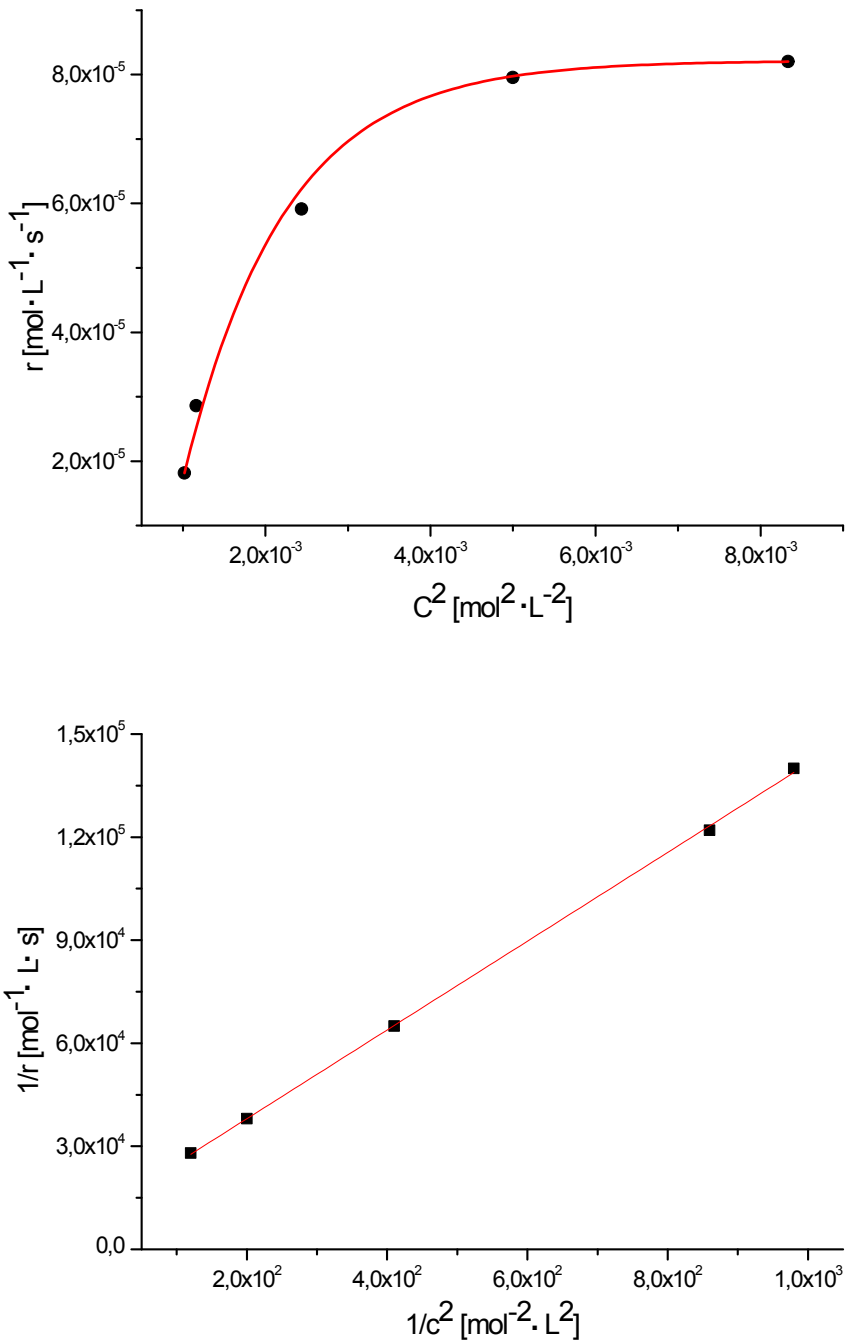

Figure S57. Kinetic plot constructed based on the Michaelis-Menten model (**top**) and the respective Lineweaver-Burk plot (**bottom**) for the reaction in the presence of cage **5** (0.5 mol%) as catalyst and 1-pyrenecarboxaldehyde (**G-6**) as the competing aromatic molecule (Figure S54), R^2 = 0.9996.

S11. ESI-MS spectra of the mixtures of 3 with G-1–G-6

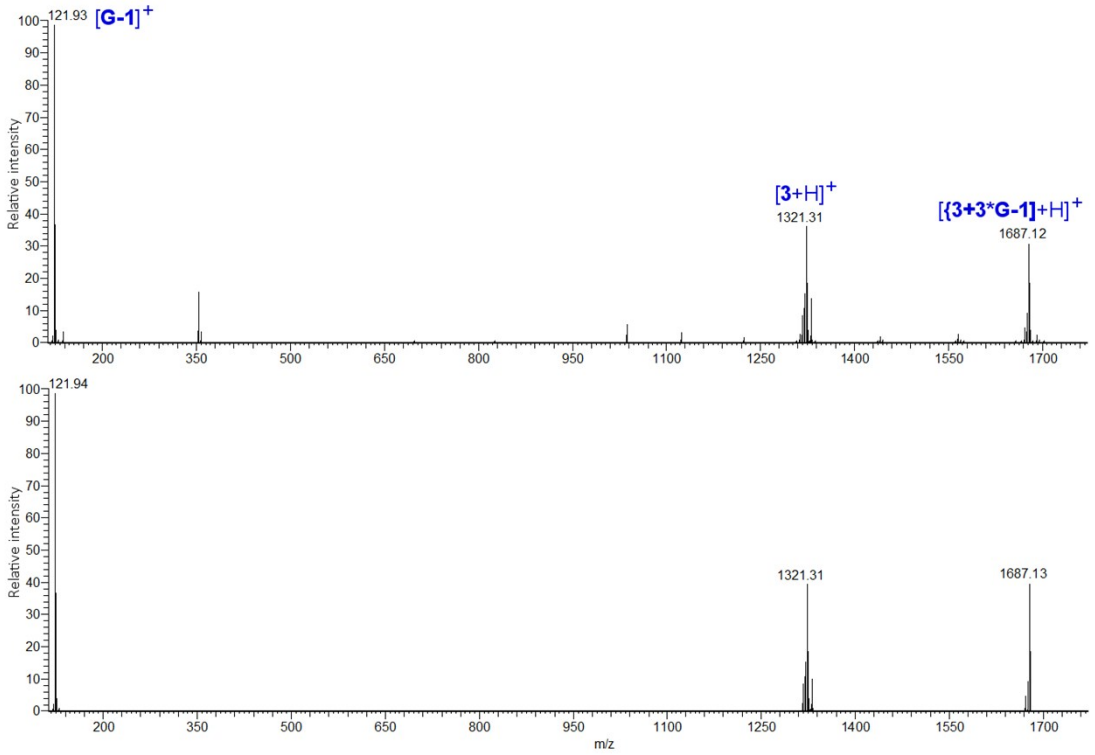

Figure S58. ESI-MS spectrum of 1:3 mol/mol mixture of **3** and **G-1**: top – measured, bottom – calculated (for the mixture comprising 1:3 non-covalent system). The peak of m/z = 1687.12 resembles to the non-covalent system (**3+3*G-1**).

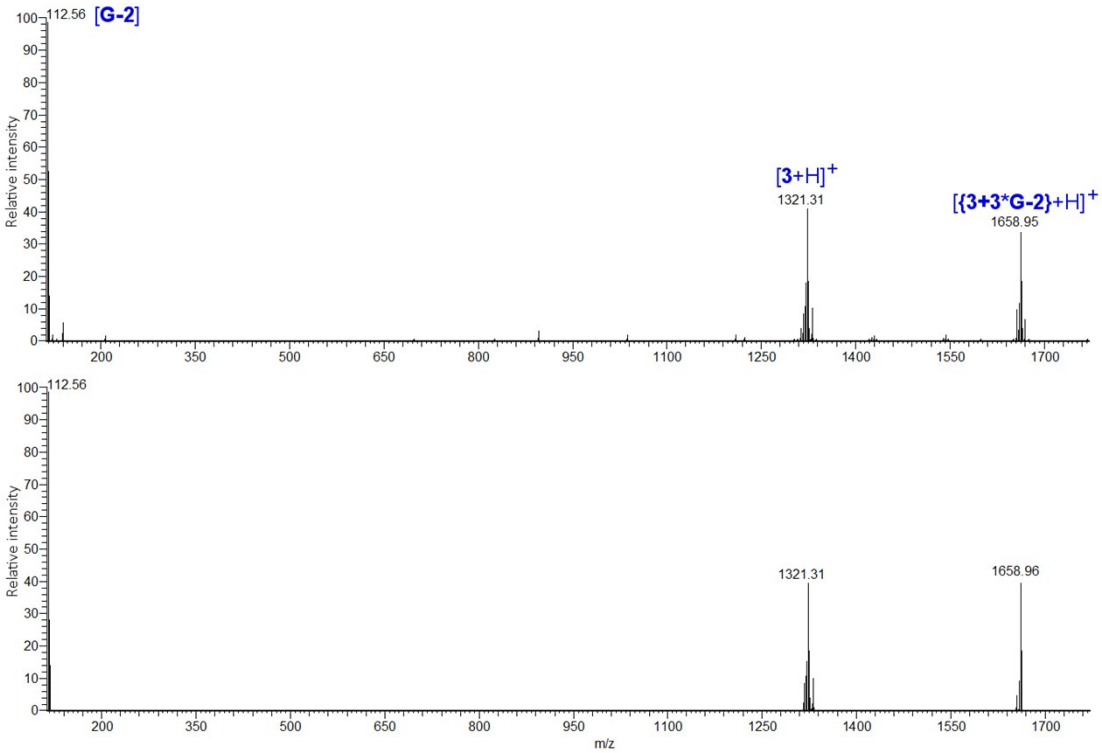

Figure S59. ESI-MS spectrum of 1:3 mol/mol mixture of **3** and **G-2**: top – measured, bottom – calculated (for the mixture comprising 1:3 non-covalent system). The peak of m/z = 1658.95 resembles to the non-covalent system (**3+3*G-2**).

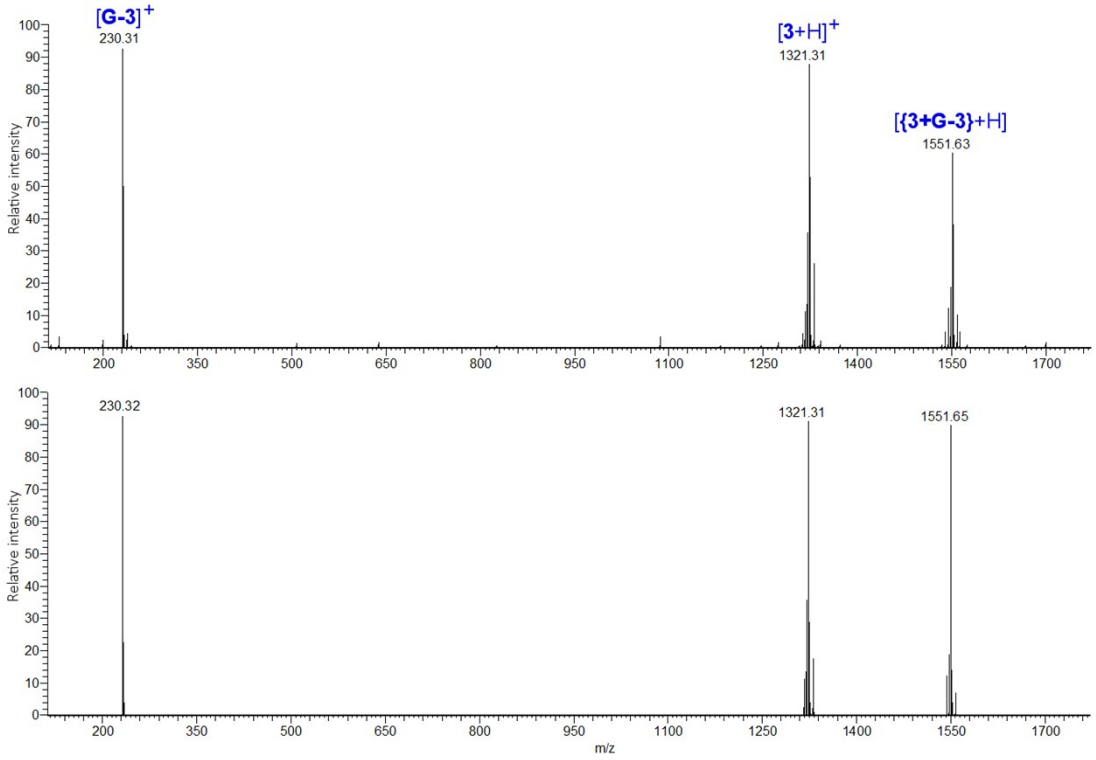

Figure S60. ESI-MS spectrum of 1:1 mol/mol mixture of **3** and **G-3**: top – measured, bottom – calculated (for the mixture comprising 1:1 non-covalent system). The peak of m/z = 1551.63 resembles to the non-covalent system (**3+G-3**).

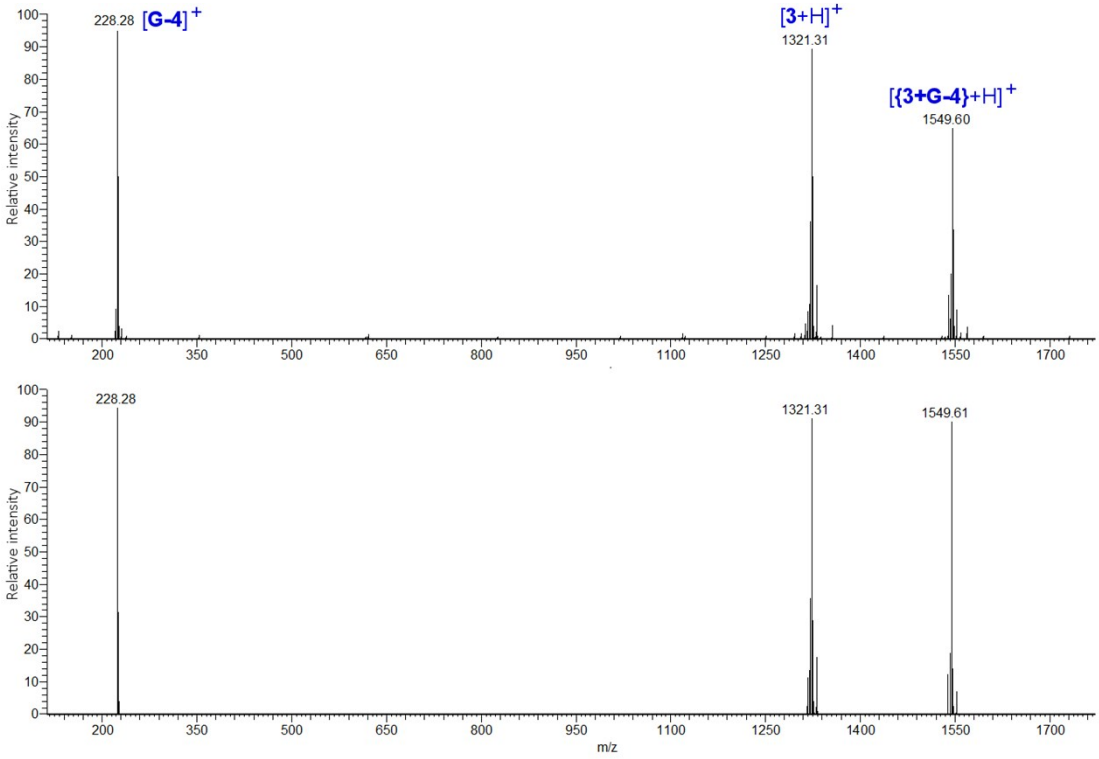

Figure S61. ESI-MS spectrum of 1:1 mol/mol mixture of **3** and **G-4**: top – measured, bottom – calculated (for the mixture comprising 1:1 non-covalent system). The peak of m/z = 1549.60 resembles to the non-covalent system (**3+G-4**).

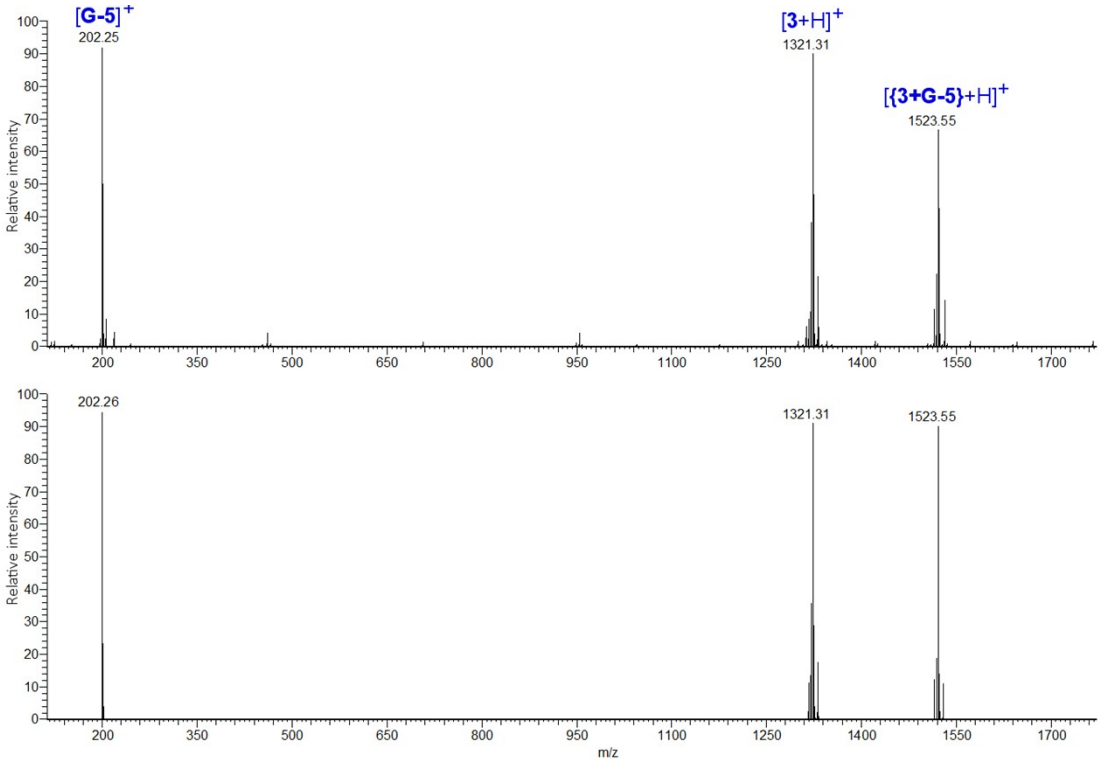

Figure S62. ESI-MS spectrum of 1:1 mol/mol mixture of **3** and **G-5**: top – measured, bottom – calculated (for the mixture comprising 1:1 non-covalent system). The peak of m/z = 1523.55 resembles to the non-covalent system (**3+G-5**).

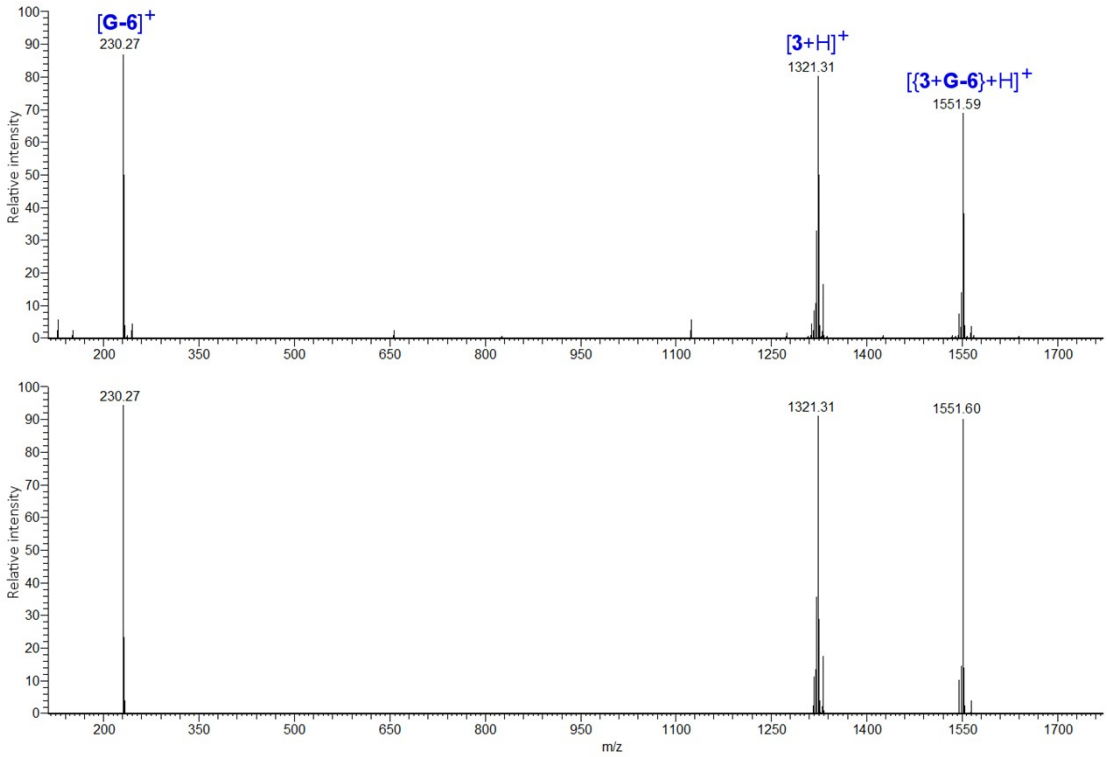

Figure S63. ESI-MS spectrum of 1:1 mol/mol mixture of **3** and **G-6**: top – measured, bottom – calculated (for the mixture comprising 1:1 non-covalent system). The peak of m/z = 1551.59 resembles to the non-covalent system (**3+G-3**).

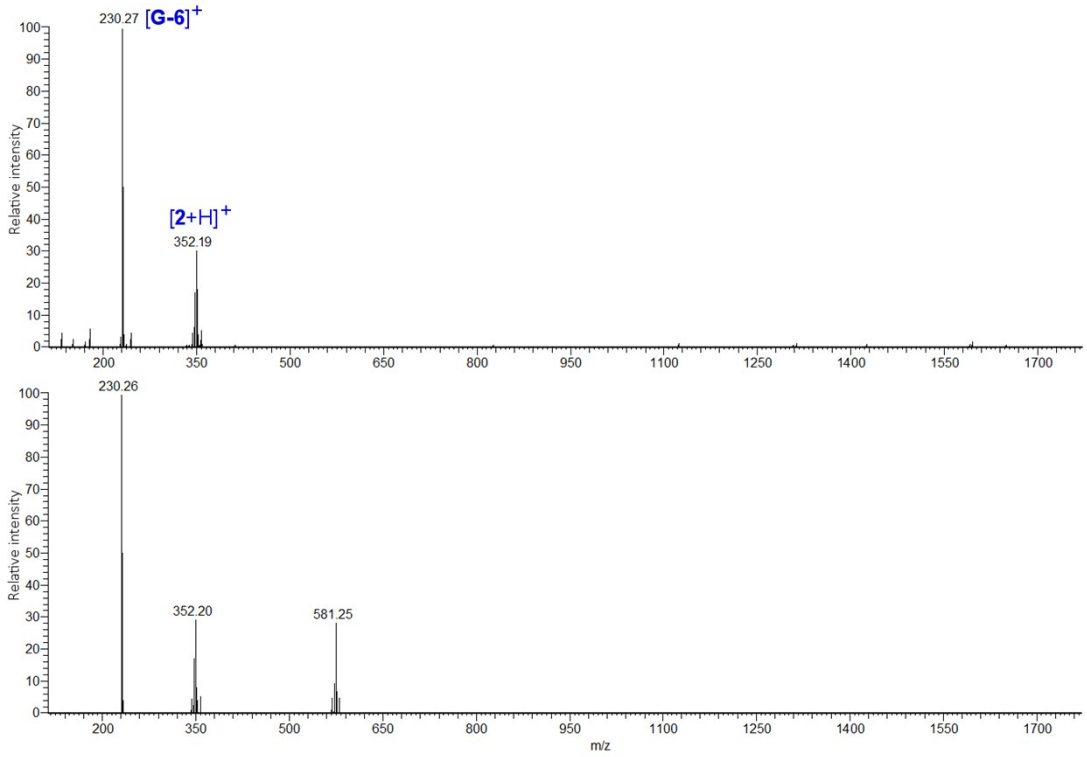

Figure S64. ESI-MS spectrum of 1:3 mol/mol mixture of **2** and **G-6**: top – measured, bottom – calculated (for the mixture comprising potential 1:1 non-covalent system: m/z = 581.25).

S12. References

[1] Wu, D. H.; Chen, A.; Johnson, C. S. *J. Magn. Reson. Ser. A* **1995**, *115*, 260–264.

[2] Jerschow, A.; Müller, N. *J. Magn. Reson.* **1997**, *125*, 372–375.

[3] Xu, W.-Q.; Fan, Y.-Z.; Wang, H.-P.; Teng, J.; Li, Y.-H.; Chen, C.-X.; Fenske, D.; Jiang, J.-J.; Su, C.-Y. *Chem. Eu. J.* **2017**, *23*, 3542-3547.

[4] Luu, H.-T.; Wiesler, S.; Frey, G.; Streuff, J. *Org. Lett*. **2015**, *17*, 2478-2481.

[5] (**a**) see data in Figure S31; (**b**) see data on reactions yields and times in Table 1, main text; (**c**) Steinborn, D. *Fundamentals of Organometallic Catalysis*; Wiley VCH, Weinheim, 2011, ISBN: 978-3-527-32717-1.

[6] Pereira, R.; Cvengroš, J. *J. Organomet. Chem.* **2013**, *729*, 81–85.

[7] *SDBSWeb: Https://Sdbs.Db.Aist.Go.Jp (National Institute of Advanced Industrial Science and Technology, Date of Access – 22.11.2019)*.

[8] Isolated yield.

[9] *CrysAlisPro Software System Ver. 171.40.53*; Rigaku OD: Oxford, UK, 2019.

[10] Sheldrick, G. M. *Acta Crystallogr. Sect. A* **2015**, *71*, 3–8.

[11] Sheldrick, G. M. *Acta Crystallogr. Sect. C* **2015**, *71*, 3–8.

[12] Dolomanov, O. V.; Bourhis, L. J.; Gildea, R. J.; Howard, J. A. K.; Puschmann, H. *J. Appl. Crystallogr.* **2009**, *42*, 339–341.

[13] Spek, A. L. *J. Appl. Crystallogr.* **2003**, *36*, 7–13.

[14] Spek, A. L. *Acta Crystallogr. Sect. C* **2015**, *71*, 9–18.

[15] Pyle, A. M.; Rehmann, J. P.; Meshoyrer, R.; Kumar, C. V.; Turro, N. J.; Barton. *J. Am. Chem. Soc*. **1989**, *111*, 3051-3058.

[16] Kasprzak, A.; Sakurai, H. *Dalton Trans*. **2019**, *48*, 17147-17152.

[17] Jullian, C.; Miranda, S.; Zapata-Torres, G.; Mendizábal, F.; Olea-Azar, C. *Bioorganic Med. Chem.* **2007**, *15*, 3217–3224.

[18] Bakkour, Y.; Vermeersch, G.; Morcellet, M.; Boschin, F.; Martel, B.; Azaroual, N. *J. Incl. Phenom.* **2006**, *54* (1–2), 109–114.

[19] Kasprzak, A.; Koszytkowska-Stawinska, M.; Nowicka, A. M.; Buchowicz, W.; Poplawska, M. *J. Org. Chem*. **2019**, *84*, 15900-15914.

[20] Jiao, J.; Li, Z.; Qiao, Z.; Li, X.; Liu, Y.; Dong, J.; Jiang, J.; Cui, Y. *Nat. Commun.* **2018**, *9*, article number 4423, 8 pages.